

COMPUTATION OF \wp -FUNCTIONS ON PLANE ALGEBRAIC CURVES

J BERNATSKA

ABSTRACT. Numerical tools for computation of \wp -functions, also known as Kleinian, or multiply periodic, are proposed. In this connection, computation of periods of the both first and second kinds is reconsidered. An analytical approach to constructing the Riemann surface of a plane algebraic curves of low gonalities is used. The approach is based on explicit radical solutions to quadratic, cubic, and quartic equations, which serve for hyperelliptic, trigonal, and tetragonal curves, respectively. The proposed analytical construction of the Riemann surface gives a full control over computation of the Abel image of any point on a curve. Therefore, computation of \wp -functions on given divisors can be done directly. An alternative computation with the help of the Jacobi inversion problem is used for verification. Hyperelliptic and trigonal curves are considered in detail, and illustrated by examples.

1. INTRODUCTION

The interest to computing \wp -functions, also known as Kleinian after [10], or multiply periodic after [3], arises from the realm of completely integrable systems, e.g. the hierarchies of the Korteweg—de Vries equation (KdV), the sine-Gordon equation (SG), the non-linear Schrödinger equation (NLS), etc., since finite-gap solutions can be expressed in terms of these functions, see [10, 6]. This representation of solutions is rarely used, and convenient tools for computation are not developed.

The only numerical computation, and graphical representation, of solutions in terms of $\wp_{1,1}$ -function can be found in [20, 21], for the mKdV equation, and the KdV equation, respectively. Since solutions are required to be real-valued, $\wp_{1,1}$ -function is computed along a particular path in the Jacobian variety. Computation of periods on a curve is avoided. Instead, $\wp_{1,1}$ -function is expressed in terms of a divisor on a hyperelliptic curve, which follows from the Jacobi inversion problem. Solving the equation is reduced to computing the Abel map by means of Euler's numerical quadrature. The required path in the Jacobian variety is constructed numerically to satisfy the reality condition for the solution.

On the other hand, solutions of completely integrable equations in term of theta functions, see for example [4], are widely used. And numerical tools for computation of the Riemann period matrix and the theta function are well developed.

A powerful method of computing first kind period matrices (normalized and not normalized) on a plane curve was presented in [12], and implemented in the Maple package `algcurves`, see a detailed description in [13]. Besides this, other packages for computing the theta function and its derivatives are created in Sage, Matlab, Julia, see for example [1].

Date: July 18, 2024.

Computation with the help of spectral approximation is suggested in [17]. Linear combinations of Chebyshev polynomials are used in approximation of integrands of first and third kind integrals between branch points, and integration is performed with the help of the orthogonality relation on the polynomials. Numerical simulation is performed in Matlab. With Riemann period matrices computed by means of this technique, solutions of the KdV and KP equations on hyperelliptic curves of genera 2, 4, 6 were computed and illustrated in [18]. Solutions of the NLS equation and the Davey–Stewartson equation on hyperelliptic curves of genera 2 and 4 were presented in [19]. The spectral approximation technique allows to increase accuracy in almost solitonic cases, when pairs of branch points collide.

The known numerical tools are designed for studying theta-functional solutions. Appropriate and convenient numerical tools are needed for computation of \wp -functions, as well. First of all, periods of the both first and second kinds are required, the latter are not covered by the known packages. The necessary second kind differentials form an associated¹ system with the standard first kind differentials. As a result, not normalized period matrices of the first and second kinds, subject to the Legendre relation, are obtained. Also a technique of computing the Abel map is needed for direct computation of \wp -functions.

In the present paper, an effective analytical method of direct computation on plane algebraic curves of low gonalities is proposed. The method is based on constructing the Riemann surface of a curve from explicit solutions obtained as radical expressions for roots of a quadratic, cubic, or quartic equation, which serve for a hyperelliptic, trigonal, or tetragonal curve, respectively. Continuous connection between these solutions can be discovered analytically. Such an analytical construction of the Riemann surface gives a full understanding how to compute the Abel image of any point on the curve.

The analytical approach was initiated by V. Enolsky, and the hyperelliptic case with real branch points was developed by him. First and second kind periods obtained by this method served for verification of relations on theta functions, and \wp -functions. However, the method had never been published before. In the present paper the method is extended to hyperelliptic curves with arbitrary complex branch points, and to trigonal curves. These two types of plane algebraic curves are the most demanded. In fact, only integrable systems with hyperelliptic spectral curves have been considered in the literature when computation arose.

In addition to direct computation of \wp -functions, computation based on the Jacobi inversion problem is also presented. The latter is used for verification that obtained values of \wp -functions are correct, as well as periods used for computing \wp -functions serve for the curve in question. In the hyperelliptic case, generalizations of the Bolza formulas, which give expressions for branch points in terms of theta functions with characteristics, are used for verification of computed periods.

The paper is organized as follows. In Preliminaries the notion of Sato weight, the definitions of the sigma function and \wp -functions are given, and also the Bolza formulas, and solutions of the Jacobi inversion problem on hyperelliptic and trigonal curves. In section 3 an analytical construction of the Riemann surface of a hyperelliptic curve, and computation of periods are explained in detail. Section 4 presents computation of the Abel image of an arbitrary point on a curve, and computation

¹Fundamental integrals of the second kind associated with the standard not normalized first kind integrals were introduced in [2, Art. 138].

of \wp -functions on non-special divisors. In sections 5, and 6 the same results are presented in the case of a trigonal curve.

The proposed method is illustrated by examples: hyperelliptic curves of genus 4 with (1) complex branch points, and (2) all real branch points, and a trigonal curve of genus 3. Computations are made in Wolfram Mathematica 12. Integrals between branch points are computed with the help of `NIntegrate` with `WorkingPrecision` of 18. The theta function is approximated by partial sums of (6), $n_i \leq 5$ is sufficient.

In almost solitonic cases the accuracy of computations with `NIntegrate` decreases sufficiently, and the spectral approximation technique can be applied to improve the situation.

2. PRELIMINARIES

2.1. Sato weight. The notion of *Sato weight* plays an important role in the theory of (n, s) -curves. Such a curve arises as a universal unfolding of the Pham singularity $y^n + x^s = 0$ with co-prime n and s , $n < s$. Thus, an (n, s) -curve is defined by the equation

$$(1a) \quad \mathcal{C} = \{(x, y) \in \mathbb{C}^2 \mid f(x, y) = 0\},$$

$$(1b) \quad f(x, y) = -y^n + x^s + \sum_{j=0}^{n-2} \sum_{i=0}^{s-2} \lambda_{ns-in-js} y^j x^i,$$

$$(1c) \quad \lambda_{k \leq 0} = 0, \quad \lambda_k \in \mathbb{C}.$$

where λ_k serve as parameters of the curve, and k shows the Sato weight of λ_k . Only parameters with positive Sato weights are allowed. The Sato weights of x and y are $\text{wgt } x = n$, and $\text{wgt } y = s$. Then $\text{wgt } f(x, y) = ns$. Note, that some terms are omitted in (1), since the definition contains the minimal number of parameters. All extra terms can be eliminated by a proper bi-rational transformation.

Due to n and s are co-prime, infinity is a Weierstrass point where all n sheets of the curve join. Let ξ denote a local parameter near infinity, then

$$(2) \quad x = \xi^{-n}, \quad y = \xi^{-s}(1 + O(\lambda))$$

gives the simplest parametrization of (1). Evidently, the Sato weight equals the opposite to the exponent of the leading term in the expansion near infinity.

2.2. Abel map. Let $du = (du_{\mathfrak{w}_1}, du_{\mathfrak{w}_2}, \dots, du_{\mathfrak{w}_g})^t$ be not normalized first kind differentials, labeled by elements of the Weierstrass gap sequence $\{\mathfrak{w}_1, \mathfrak{w}_2, \dots, \mathfrak{w}_g\}$, which coincide with negative Sato weights: $\text{wgt } du_{\mathfrak{w}_i} = -\mathfrak{w}_i$, and show the orders of zero at infinity.

Let the Abel map \mathcal{A} be constructed with not normalized differentials du :

$$(3) \quad \mathcal{A}(P) = \int_{\infty}^P du, \quad P = (x, y) \in \mathcal{C}.$$

Here infinity is used as the base point, which is the standard choice in the case of (n, s) -curves. If a curve is not an (n, s) -one, the base point is chosen among Weierstrass points on the curve.

First kind integrals along canonical homology cycles $\{\mathfrak{a}_i, \mathfrak{b}_i\}_{i=1}^g$ give first kind period matrices:

$$(4) \quad \omega = (\omega_{ij}) = \left(\int_{\mathfrak{a}_j} du_i \right), \quad \omega' = (\omega'_{ij}) = \left(\int_{\mathfrak{b}_j} du_i \right).$$

Columns of ω, ω' generate the lattice \mathfrak{P} of periods. Then $\text{Jac}(\mathcal{C}) = \mathbb{C}^g \setminus \mathfrak{P}$ is the Jacobian variety of the curve \mathcal{C} .

Let $v = \omega^{-1}u$ be normalized coordinates on the Jacobian variety, and $(1_g, \tau)$ be normalized periods, where 1_g denotes the identity matrix of size g , and $\tau = \omega^{-1}\omega'$. Matrix τ is symmetric with a positive imaginary part: $\tau^t = \tau$, $\text{Im } \tau > 0$, that is τ belongs to the Siegel upper half-space. The normalised first kind differentials are defined by

$$dv = \omega^{-1}du,$$

and the Abel map $\bar{\mathcal{A}}$ with respect to the normalized differentials is

$$(5) \quad \bar{\mathcal{A}}(P) = \int_{\infty}^P dv, \quad P = (x, y) \in \mathcal{C}.$$

2.3. Theta and sigma functions. Recall the two entire functions on $\mathbb{C}^g \supset \text{Jac}(\mathcal{C})$, which generate multiply periodic (or Abelian) functions, and so serve for uniformization of a curve \mathcal{C} .

The Riemann *theta function*

$$(6) \quad \theta(v; \tau) = \sum_{n \in \mathbb{Z}^g} \exp(\iota\pi n^t \tau n + 2\iota\pi n^t v)$$

is defined in terms of normalized coordinates v , and normalized period matrix τ . A theta function with characteristic is defined by

$$(7) \quad \theta[\varepsilon](v; \tau) = \exp\left(\iota\pi\left(\frac{1}{2}\varepsilon'^t\right)\tau\left(\frac{1}{2}\varepsilon'\right) + 2\iota\pi\left(v + \frac{1}{2}\varepsilon\right)^t\left(\frac{1}{2}\varepsilon'\right)\right)\theta\left(v + \frac{1}{2}\varepsilon + \tau\left(\frac{1}{2}\varepsilon'\right); \tau\right),$$

where a characteristic is a $2 \times g$ matrix $[\varepsilon] = (\varepsilon', \varepsilon)^t$ with real values within the interval $[0, 2)$. Every point u in the fundamental domain of $\text{Jac}(\mathcal{C})$ can be represented by its characteristic $[\varepsilon]$, namely

$$u = \frac{1}{2}\omega\varepsilon + \frac{1}{2}\omega'\varepsilon'.$$

In the hyperelliptic case, the Abel images of branch points and any combination of branch points are described by characteristics with components 1 or 0, which are called half-integer characteristics. Such a characteristic is odd whenever $\varepsilon^t\varepsilon' = 0 \pmod{2}$, and even whenever $\varepsilon^t\varepsilon' = 1 \pmod{2}$. A theta function with half-integer characteristic has the same parity as its characteristic.

The modular invariant entire function on $\text{Jac}(\mathcal{C})$ is called the *sigma function*. As a definition we use its relation with the theta function:

$$(8) \quad \sigma(u) = C \exp\left(-\frac{1}{2}u^t \varkappa u\right) \theta[K](\omega^{-1}u; \omega^{-1}\omega'),$$

where $[K]$ denotes the characteristic of the vector of Riemann constants, and $\varkappa = \eta\omega^{-1}$ is a symmetric matrix obtained from second kind periods η . The Sato weight of the sigma function is $\text{wgt } \sigma = -(n^2 - 1)(s^2 - 1)/24$, see [9].

The sigma function is defined in terms of not normalized coordinates u , and not normalized period matrices of the first kind ω, ω' , and of the second kind η, η' . The latter are defined as follows

$$(9) \quad \eta = (\eta_{ij}) = \left(\int_{\mathfrak{a}_j} dr_i \right), \quad \eta' = (\eta'_{ij}) = \left(\int_{\mathfrak{b}_j} dr_i \right),$$

with second kind differentials $dr = (dr_{\mathfrak{w}_1}, dr_{\mathfrak{w}_2}, \dots, dr_{\mathfrak{w}_g})^t$. It is important to choose the second kind differentials which form an associated system with differentials of the first kind, see [2, Art. 138]. Note that $dr_{\mathfrak{w}_i}$ has the only pole of order \mathfrak{w}_i

at infinity, and so $\text{wgt } r_{\mathfrak{w}_i} = \mathfrak{w}_i$. In the vicinity of infinity, $\xi(\infty) = 0$, the following relation holds

$$(10) \quad \text{res}_{\xi=0} \left(\int_0^\xi du(\tilde{\xi}) \right) dr(\xi)^t = 1_g,$$

which completely determines the principle part of $dr(\xi)$.

The not normalized periods matrices of the first ω, ω' and second η, η' kinds satisfy the Legendre relation

$$(11) \quad \Omega^t J \Omega = 2\pi i J, \\ \Omega = \begin{pmatrix} \omega & \omega' \\ \eta & \eta' \end{pmatrix}, \quad J = \begin{pmatrix} 0 & -1_g \\ 1_g & 0 \end{pmatrix}.$$

Multiply periodic \wp -functions are defined with the help of the sigma function:

$$\wp_{i,j}(u) = -\frac{\partial^2 \log \sigma(u)}{\partial u_i \partial u_j}, \quad \wp_{i,j,k}(u) = -\frac{\partial^3 \log \sigma(u)}{\partial u_i \partial u_j \partial u_k}.$$

From (8) we obtain expressions in terms of the theta function:

$$(12) \quad \begin{aligned} \wp_{i,j}(u) &= \varkappa_{i,j} - \frac{\partial^2}{\partial u_i \partial u_j} \log \theta[K](\omega^{-1}u; \omega^{-1}\omega'), \\ \wp_{i,j,k}(u) &= -\frac{\partial^3}{\partial u_i \partial u_j \partial u_k} \log \theta[K](\omega^{-1}u; \omega^{-1}\omega'). \end{aligned}$$

The vector of Riemann constants K with respect to a base point P_0 is defined by the formula, [14, Eq. (2.4.14)]

$$(13) \quad K_j = \frac{1}{2}(1 + \tau_{j,j}) - \sum_{l \neq j} \oint_{\mathfrak{a}_l} dv_j(P) \int_{P_0}^P dv_l, \quad j = 1, \dots, g.$$

In the hyperelliptic case, the vector is computed² in [16, p. 14], and equals the sum of all odd characteristics of the fundamental set of $2g + 1$ characteristics which represent branch points, according to [2, Art.200–202].

2.4. Bolza formulas and generalizations. In genus 2, expressions for branch points in terms of the theta function are known as the Bolza formulas

$$e_\iota = -\frac{\partial_{u_3} \theta[\{\iota\}](\omega^{-1}u)}{\partial_{u_1} \theta[\{\iota\}](\omega^{-1}u)} \Big|_{u=0},$$

where $[\{\iota\}]$ denotes the characteristic corresponding to a branch point e_ι , see [8, Eq. (6)]. A generalization of the Bolza formulas for a hyperelliptic curve of arbitrary genus g is obtained in [5]. In particular,

$$e_\iota = -\frac{\partial_{u_{2(g \bmod 2)+1}, \dots, u_{2g-7}, u_{2g-1}}^{[g/2]} \theta[\{\iota\}](\omega^{-1}u)}{\partial_{u_{2(g \bmod 2)+1}, \dots, u_{2g-7}, u_{2g-3}}^{[g/2]} \theta[\{\iota\}](\omega^{-1}u)} \Big|_{u=0}.$$

²We use a homology basis different from [16], and so $[K]$ is not exactly the same, but computed in a similar way.

2.5. Jacobi inversion problem. Given a point u of the Jacobian variety $\text{Jac}(\mathcal{C})$ find a reduced divisor $D \in \mathcal{C}^g$ such that $\mathcal{A}(D) = u$. Every class of linearly equivalent divisors on a curve of genus g has a representative of degree g or less, which is called a reduced divisor. Reduced divisors of degree less than g are special, and $\theta[K]$ vanishes on such divisors, according to the Riemann vanishing theorem. Reduced divisors of degree g are non-special. Every non-special divisor represents its class uniquely.

A solution of the Jacobi inversion problem is known for non-special divisors. On hyperelliptic curves such a solution was given in [2, Art. 216] and rediscovered in [10, Theorem 2.2]. Let a non-degenerate hyperelliptic curve of genus g be defined³ by

$$(14) \quad -y^2 + x^{2g+1} + \sum_{i=1}^{2g} \lambda_{2i+2} x^{2g-i} = 0.$$

Let $u = \mathcal{A}(D)$ be the Abel image of a degree g positive non-special divisor D on the curve. Then D is uniquely defined by the system of equations

$$(15a) \quad \mathcal{R}_{2g}(x; u) \equiv x^g - \sum_{i=1}^g x^{g-i} \wp_{1,2i-1}(u) = 0,$$

$$(15b) \quad \mathcal{R}_{2g+1}(x, y; u) \equiv 2y + \sum_{i=1}^g x^{g-i} \wp_{1,1,2i-1}(u) = 0.$$

On a trigonal curve, the Jacobi inversion problem is solved in [11]. A method of obtaining such a solution on a curve of an arbitrary gonality is presented in [7]; trigonal, tetragonal and pentagonal curves are considered as an illustration. In the case of a $(3, 3m + 1)$ -curve, a degree g positive non-special divisor D such that $u = \mathcal{A}(D)$ is given by the system

$$(16a) \quad \mathcal{R}_{6m+1}(x, y; u) \equiv x^{2m} - y \sum_{i=1}^m \wp_{1,3i-2}(u) x^{m-i} - \sum_{i=1}^{2m} \wp_{1,3i-1}(u) x^{2m-i} = 0,$$

$$(16b) \quad \begin{aligned} \mathcal{R}_{6m+2}(x, y; u) \equiv & 2yx^m + y \sum_{i=1}^m (\wp_{1,1,3i-2}(u) - \wp_{2,3i-2}(u)) x^{m-i} \\ & + \sum_{i=1}^{2m} (\wp_{1,1,3i-1}(u) - \wp_{2,3i-1}(u)) x^{2m-i} = 0. \end{aligned}$$

In the case of a $(3, 3m + 2)$ -curve, by the system

$$(17a) \quad \mathcal{R}_{6m+2}(x, y; u) \equiv yx^m - y \sum_{i=1}^m \wp_{1,3i-1}(u) x^{m-i} - \sum_{i=1}^{2m+1} \wp_{1,3i-2}(u) x^{2m+1-i} = 0,$$

$$(17b) \quad \mathcal{R}_{6m+3}(x, y; u) \equiv 2x^{2m+1} + y \sum_{i=1}^m (\wp_{1,1,3i-1}(u) - \wp_{2,3i-1}(u)) x^{m-i}$$

³A $(2, 2g + 1)$ -curve serves as a canonical form of hyperelliptic curves of genus g .

$$-\sum_{i=1}^{2m+1} (\wp_{1,1,3i-2}(u) - \wp_{2,3i-2}(u)) x^{2m+1-i} = 0.$$

3. PERIODS ON A HYPERELLIPTIC CURVE

Hyperelliptic curves are the best known plane algebraic curves. There exists a universal approach to choosing a homology and cohomology basis, as well as constructing the Riemann surface.

3.1. Hyperelliptic curves. Let a generic hyperelliptic curve be defined by

$$(18) \quad 0 = f(x, y) = -y^2 + y\mathcal{Q}(x) + \mathcal{P}(x),$$

where $\deg \mathcal{P} = 2g + 1$ or $2g + 2$, in the case of genus g .

An equation with $\deg \mathcal{P} = 2g + 1$, $\mathcal{Q}(x) \equiv 0$ defines an (n, s) -curve, which is considered as the canonical form of a hyperelliptic curve of genus g :

$$0 = f(x, y) = -y^2 + x^{2g+1} + \lambda_4 x^{2g-1} + \cdots + \lambda_{4g} x + \lambda_{4g+2}.$$

Sato weights are $\text{wgt } x = 2$, $\text{wgt } y = 2g + 1$, and so $\text{wgt } f = 4g + 2$. The term $\lambda_2 x^{2g}$ of a generic \mathcal{P} is eliminated by a proper Möbius transformation, and $y\mathcal{Q}(x)$ is eliminated by the map $y \mapsto \tilde{y} + \frac{1}{2}\mathcal{Q}(x)$, which leads to

$$0 = f(x, \tilde{y}) = -\tilde{y}^2 + \tilde{\mathcal{P}}(x), \quad \tilde{\mathcal{P}}(x) = \mathcal{P}(x) + \frac{1}{4}\mathcal{Q}(x)^2.$$

Thus, the discriminant of (18) is defined by the formula

$$(19) \quad \Delta(x) = \tilde{\mathcal{P}}(x) = \mathcal{P}(x) + \frac{1}{4}\mathcal{Q}(x)^2.$$

A canonical curve can be defined by its branch points $\{(e_i, 0)\}_{i=1}^{2g+1}$, namely

$$(20) \quad 0 = f(x, y) = -y^2 + \mathcal{P}(x), \quad \mathcal{P}(x) = \prod_{j=1}^{2g+1} (x - e_j).$$

For the sake of brevity, the notation e_i is employed both for a branch point $(e_i, 0)$ and its x -coordinate, in the hyperelliptic case. If all branch points are distinct, then the curve is non-degenerate, and its genus equals g . The curve (20) has also a branch point located at infinity, referred also as e_0 . If $\sum_{i=1}^{2g+1} e_i = 0$, then $\lambda_2 = 0$. However, we omit the latter condition, and allow $\{e_i\}$ be arbitrary.

A curve with $\deg \mathcal{P} = 2g + 2$, and $\mathcal{Q}(x) \equiv 0$ has $2g + 2$ finite branch points, denoted by $\{(e_i, 0)\}_{i=0}^{2g+1}$. The corresponding canonical form is obtained by moving the finite branch point e_0 to infinity.

In the generic case (18), the maximal $\deg \mathcal{Q}$ equals g , which respects the Sato weight, and guarantees that the genus of a curve does not exceed g . Such a curve can be defined by choosing arbitrary values $\{e_i\}$ of number $2g + 1$ or $2g + 2$, and choosing a polynomial \mathcal{Q} of degree up to g . Then the corresponding y -coordinates of branch points $\{(e_i, h_i)\}$ are obtained by the formula $h_i = \frac{1}{2}\mathcal{Q}(e_i)$.

The Weierstrass gap sequence on a hyperelliptic curve (18) is

$$\mathfrak{W} = \{\mathfrak{w}_i = 2i - 1 \mid i = 1, \dots, g\}.$$

In what follows, we focus on the canonical form of a hyperelliptic curve.

3.2. Riemann surface. At every point x , except branch points, there exist two values of y ($s = \pm 1$):

$$(21a) \quad y_s(x) = s\sqrt{\Delta(x)}, \quad \Delta(x) = \mathcal{P}(x), \quad \text{in the canonical case,} \quad \text{or}$$

$$(21b) \quad y_s(x) = \frac{1}{2}\mathcal{Q}(x) + s\sqrt{\Delta(x)}, \quad \text{in the generic case.}$$

Let the square root function be defined as follows

$$(22) \quad \sqrt{\Delta(x)} = \begin{cases} \sqrt{|\Delta(x)|} e^{(\imath/2)\arg \Delta(x)} & \text{if } \arg \Delta(x) \geq 0, \\ \sqrt{|\Delta(x)|} e^{(\imath/2)\arg \Delta(x) + \imath\pi} & \text{if } \arg \Delta(x) < 0, \end{cases}$$

where \arg has the range $(-\pi, \pi]$. With such a definition the range of $\arg \sqrt{\Delta(x)}$ is $[0, \pi)$. Moreover,

Theorem 1. *Let $\sqrt{\Delta}$ be defined by (22). Then y_s defined by (21) have discontinuity over the contour $\Gamma = \{x \mid \arg \Delta(x) = 0\}$, and y_+ serves as the analytic continuation of y_- on the other side of the contour, and vice versa.*

Proof. Let \tilde{x} be located in the vicinity of the contour Γ , more precisely $|\arg \Delta(\tilde{x})| < 2\phi$, with a small positive value ϕ . Then $0 \leq \arg \sqrt{\Delta(\tilde{x})} < \phi$ if $\arg \Delta(\tilde{x}) \geq 0$, and $\pi - \phi < \arg \sqrt{\Delta(\tilde{x})} < \pi$ if $\arg \Delta(\tilde{x}) < 0$. Evidently, the discontinuity of $\sqrt{\Delta}$ is located over the contour Γ .

Next, we find the analytic continuation of $\sqrt{\Delta}$. Let $U(x_0; \delta)$ be a disc of radius δ with the center at $x_0 \in \Gamma$. The contour Γ divides the disc into two parts: U_+ where $\arg \Delta(x) \geq 0$, and U_- where $\arg \Delta(x) < 0$. The analytic continuation of $\sqrt{\Delta}$ from U_+ to U_- is given by $-\sqrt{\Delta}$, since the range of $\arg(-\sqrt{\Delta(x)}) = \arg(e^{-\imath\pi}\sqrt{\Delta(x)})$ is $[-\pi, 0)$. And the analytic continuation of $\sqrt{\Delta}$ from U_- to U_+ is given by $-\sqrt{\Delta} = e^{\imath\pi}\sqrt{\Delta}$. \square

With the help of definition (22), we fix the position of discontinuity of $\sqrt{\Delta}$ at the contour Γ . This allows to determine connection of solutions y_s on the Riemann surface, and mark sheets.

In order to construct the Riemann surface of a curve, we choose a continuous path on the Riemann sphere through all $\{e_i\}$, and lift it to each sheet of the curve. Along this path, at any intersection with Γ the sign s in (21) changes into the opposite. In this way the sheets are marked.

3.3. Continuous path. Choosing a continuous path is the *key element* of the proposed scheme of analytic constructing a Riemann surface. The path starts at infinity as $x \rightarrow -\infty$, goes through all branch points in the chosen order, and ends at infinity as $x \rightarrow \infty$. Below, an algorithm of drawing such a path and marking sheets is presented.

1. Let all finite branch points $\{e_i\}_{i=1}^{2g+1}$ be sorted ascendingly first by the real part, then the imaginary part.
2. According to this order a path on the Riemann sphere through all e_i is constructed from straight line segments $[e_i, e_{i+1}]$, $i = 1, \dots, 2g$. Then the segment $(-\infty, e_1]$ is added at the beginning of the polygonal path, and $[e_{2g+1}, \infty)$ at the end. The path goes below the points $\{e_i\}$, and so in the counter-clockwise direction near each e_i . Such a path is marked in orange on fig. 2.

3. Plot the contour $\Gamma = \{x \mid \arg \mathcal{P}(x) = 0\}$, which consists of segments Γ_i between e_i and infinity, see blue contours on fig. 2. Find the sequence of signs $\{\mathbf{s}_{0,1}\} \cup \{\mathbf{s}_{i,i+1}\}_{i=1}^{2g} \cup \{\mathbf{s}_{2g+1,0}\}$ on each segment of the path, starting with $\mathbf{s}_{0,1} = +1$. Index 0 is used for infinity. At any intersection with Γ the sign changes into the opposite. The sequence of signs determines connection between solutions y_s on Sheet a. Sheet b is marked by the sequence with opposite signs on each segment. On a hyperelliptic curve, Sheet a is sufficient for all computations.

3.4. Homology. Cuts are made between points e_{2k-1} and e_{2k} with k from 1 to g , and from e_{2g+1} to infinity ∞ . With k running from 1 to g an \mathbf{a}_k -cycle encircles the cut (e_{2k-1}, e_{2k}) counter-clockwise, and a \mathbf{b}_k -cycle enters into the cut (e_{2k-1}, e_{2k}) and emerges from the cut (e_{2g+1}, ∞) , see fig. 1 as an example. This canonical homology basis is adopted from Baker [2, p. 303], and can be considered as standard on a hyperelliptic curve.

Remark 1. In the case of $\deg \mathcal{P} = 2g+2$, with branch points $\{(e_i, 0)\}_{i=0}^{2g+1}$, we sort the latter in the same way as in the canonical case. So e_0 has the smallest real and imaginary parts among all branch points. Cuts are made between points e_{2k-1} and e_{2k} with k from 1 to g , and from e_{2g+1} to e_0 through infinity. A canonical homology basis is introduced in a similar way: an \mathbf{a}_k -cycle encircles the cut (e_{2k-1}, e_{2k}) counter-clockwise, and a \mathbf{b}_k -cycle enters into the cut (e_{2k-1}, e_{2k}) and emerges from the cut $e_{2g+1}-\infty-e_0$.

3.5. Cohomology. First kind differentials are defined in the standard way, see [2, p. 306] for example,

$$(23) \quad du_{2i-1} = \frac{x^{g-i} dx}{\partial_y f(x, y)}, \quad i = 1, \dots, g.$$

On the canonical hyperelliptic curve, the second kind differentials associated with the first kind ones have the form

$$(24) \quad dr_{2i-1} = \frac{dx}{\partial_y f(x, y)} \sum_{k=1}^{2i-1} k \lambda_{4i-2k+2} x^{g-i+k}, \quad i = 1, \dots, g.$$

3.6. Computation of periods. First kind integrals on each segment along the polygonal path lifted to Sheet a are computed:

$$(25a) \quad \mathcal{A}_{i,i+1}^{[\mathbf{s}_{i,i+1}]} = \int_{e_i}^{e_{i+1}} du^{[\mathbf{s}_{i,i+1}]}, \quad i = 1, \dots, 2g,$$

$$(25b) \quad \mathcal{A}_{0,1}^{[\mathbf{s}_{0,1}]} = \int_{-\infty}^{e_1} du^{[\mathbf{s}_{0,1}]}, \quad \mathcal{A}_{2g+1,0}^{[\mathbf{s}_{2g+1,0}]} = \int_{e_{2g+1}}^{\infty} du^{[\mathbf{s}_{2g+1,0}]}.$$

The integrand of $\mathcal{A}_{i,j}^{[\mathbf{s}_{i,j}]}$ is taken with the sign $\mathbf{s}_{i,j}$, that is

$$du^{[\mathbf{s}_{i,j}]} = \begin{pmatrix} x^{g-1} \\ \vdots \\ x \\ 1 \end{pmatrix} \frac{dx}{-2 \mathbf{s}_{i,j} \sqrt{\mathcal{P}(x)}}.$$

Due to the involution of a hyperelliptic curve, the following relations hold

$$(26) \quad \sum_{k=1}^g \mathcal{A}_{2k-1,2k}^{[s_{2k-1,2k}]} + \mathcal{A}_{2g+1,0}^{[s_{2g+1,0}]} = 0, \quad \mathcal{A}_{0,1}^{[s_{0,1}]} + \sum_{k=1}^g \mathcal{A}_{2k,2k+1}^{[s_{2k,2k+1}]} = 0,$$

which serve for verification.

According to the choice of canonical cycles, columns of the first kind period matrices are

$$(27) \quad \omega_k = 2\mathcal{A}_{2k-1,2k}^{[s_{2k-1,2k}]}, \quad \omega'_k = -2 \sum_{j=k}^g \mathcal{A}_{2j,2j+1}^{[s_{2j,2j+1}]}.$$

The normalized period matrix is obtain by

$$\tau = \omega^{-1} \omega',$$

and required to be symmetric with positive imaginary part.

Second kind integrals $\mathcal{B}_{i,j}^{[s_{i,j}]}$ are computed similarly:

$$\mathcal{B}_{i,j}^{[s_{i,j}]} = \int_{e_i}^{e_j} dr^{[s_{i,j}]},$$

where $dr^{[s_{i,j}]}$, defined by (24), is taken with the sign $s_{i,j}$. Then the second kind period matrices are

$$(28) \quad \eta_k = 2\mathcal{B}_{2k-1,2k}^{[s_{2k-1,2k}]}, \quad \eta'_k = -2 \sum_{j=k}^g \mathcal{B}_{2j,2j+1}^{[s_{2j,2j+1}]}.$$

The symmetric matrix responsible for modular invariance⁴ is

$$\varkappa = \eta \omega^{-1}.$$

The four matrices ω , ω' , η , η' satisfy the Legendre relation (11), which serve for verification.

3.7. Example 1: Arbitrary complex branch points. Let a hyperelliptic curve of genus 4 possesses the given finite branch points:

$$-18 - 2i, -16 + 5i, -11 + 3i, -10 - i, -4 + 2i, -3 + 3i, 3 + 3i, 7 - 2i, 13 - i.$$

On the other hand, this curve is defined by the equation

$$(29a) \quad 0 = f(x, y) = -y^2 + \mathcal{P}(x),$$

$$(29b) \quad \begin{aligned} \mathcal{P}(x) = & x^9 + (39 - 10i)x^8 + (217 - 288i)x^7 - (7585 - 826i)x^6 \\ & - (79138 - 82462i)x^5 + (324058 + 455846i)x^4 + (4126332 - 3930980i)x^3 \\ & - (14219032 + 29444932i)x^2 - (131012592 - 28208616i)x \\ & - 101860560 + 245519280i. \end{aligned}$$

Cuts and homology cycles, see fig. 1, are introduced as explained in subsection 3.4. On fig. 2, the contour Γ is shown in blue. Note, that the cut (e_9, ∞) coincides with segment Γ_9 . A continuous path is marked in orange. It goes below points e_i . A curved orange line near a cut shows which side of the cut is chosen. As seen on fig. 3, along the contour Γ , solution y_+ continuously connects to y_- , and vice versa.

⁴By introducing the exponential factor with \varkappa , the theta function is transformed into the modular invariant sigma function, cf. (8).

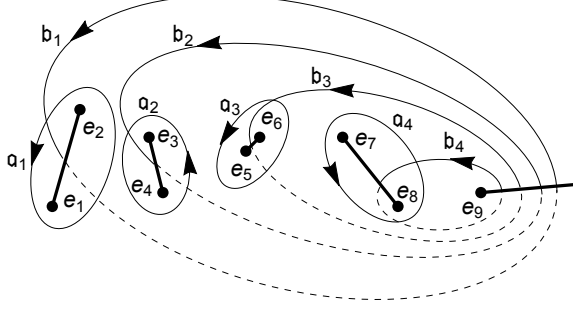
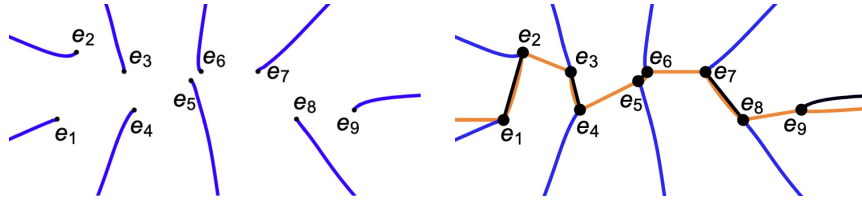
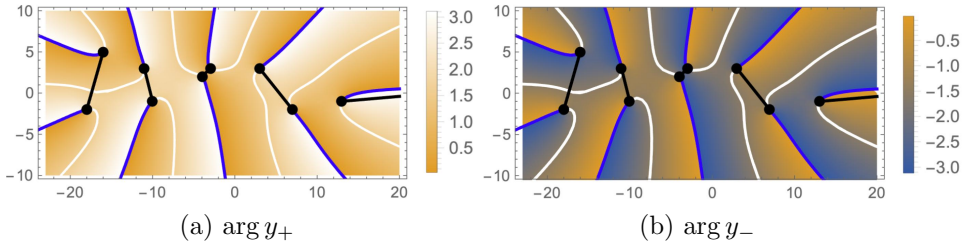
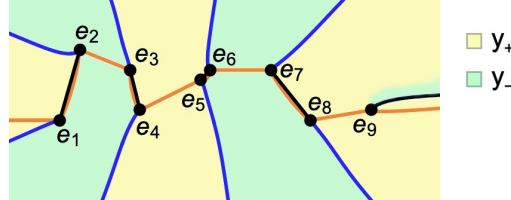


FIGURE 1. Canonical homology cycles.

FIGURE 2. The contour Γ (blue), and a continuous path (orange).FIGURE 3. Density plots of $\arg y_s$, and the contour Γ (blue).

Now we mark Sheet a, see fig. 4. Let start with $s_{0,1} = +1$ on segment $(-\infty, e_1]$.

FIGURE 4. Connection of solutions y_+ and y_- on Sheet a.

The orange path intersects the blue contour at point e_1 , and so the sign changes: $s_{1,2} = -1$. The path goes along the right side of the cut (e_1, e_2) , and the sign remains the same on the next segment: $s_{2,3} = -1$. From e_3 to e_4 the path goes along the left side of the cut (e_3, e_4) , so the sign remains the same: $s_{3,4} = -1$. The

next intersection with the blue contour occurs at point e_4 , thus $s_{4,5} = +1$. And again at point e_5 , so $s_{5,6} = s_{6,7} = s_{7,8} = -1$. Once again, the path intersects the blue contour at point e_8 , thus $s_{8,9} = s_{9,0} = +1$. Finally, the sequence of signs is

$$\text{Sheet a: } \{s_{0,1}, s_{1,2}, s_{2,3}, s_{3,4}, s_{4,5}, s_{5,6}, s_{6,7}, s_{7,8}, s_{8,9}, s_{9,0}\} = \{+1, -1, -1, -1, +1, -1, -1, -1, +1, +1\}.$$

Along segment Γ_9 solution y_+ on Sheet a connects to y_- on Sheet b, the latter is shown in green in the vicinity of Γ_9 , see fig. 4.

First kind differentials as functions of x are

$$du^{[s]} = \begin{pmatrix} x^3 \\ x^2 \\ x \\ 1 \end{pmatrix} \frac{dx}{-2s\sqrt{P(x)}}.$$

According to the picture of homology cycles, see fig. 1, the first kind period matrices ω and ω' are computed as follows

$$\begin{aligned} \omega &= 2(\mathcal{A}_{1,2}^{[-]}, \mathcal{A}_{3,4}^{[-]}, \mathcal{A}_{5,6}^{[-]}, \mathcal{A}_{7,8}^{[-]}), \\ \omega' &= -2(\mathcal{A}_{2,3}^{[-]} + \mathcal{A}_{4,5}^{[+]}) + \mathcal{A}_{6,7}^{[-]} + \mathcal{A}_{8,9}^{[+]}, \mathcal{A}_{4,5}^{[+]}, \mathcal{A}_{6,7}^{[-]} + \mathcal{A}_{8,9}^{[+]}, \mathcal{A}_{6,7}^{[-]} + \mathcal{A}_{8,9}^{[+]}, \mathcal{A}_{8,9}^{[+]}) \end{aligned}$$

On the curve (29) we have

$$\begin{aligned} \omega &\approx \begin{pmatrix} -1.303573 + 0.207439i & 0.848115 - 0.306788i \\ 0.073367 - 0.003075i & -0.083799 + 0.019801i \\ -0.003985 - 0.000333i & 0.008037 - 0.001042i \\ 0.000208 + 0.000046i & -0.000751 + 0.000028i \\ 0.0166625 + 0.063503i & -0.035439 - 0.017840i \\ 0.005372 - 0.014707i & -0.007363 - 0.005200i \\ -0.003023 + 0.002108i & -0.001651 - 0.000958i \\ 0.000856 + 0.000006i & -0.000350 - 0.000098i \end{pmatrix}, \\ \omega' &\approx \begin{pmatrix} -0.604960 - 0.930374i & -0.085127 + 0.237963i \\ 0.029948 + 0.024444i & 0.019758 - 0.067832i \\ -0.001525 - 0.000835i & -0.002854 + 0.005901i \\ 0.000078 + 0.000029i & 0.000324 - 0.000426i \\ 0.042341 - 0.110642i & 0.047121 - 0.129831i \\ 0.011312 - 0.018512i & 0.006638 - 0.011849i \\ -0.002257 - 0.001647i & 0.000894 - 0.001058i \\ 0.000178 + 0.000796i & 0.000117 - 0.000089i \end{pmatrix}. \end{aligned}$$

The corresponding normalized period matrix from the Siegel upper half-space is

$$\tau \approx \begin{pmatrix} 0.416960 + 1.348235i & -0.019631 + 0.866637i \\ -0.019631 + 0.866637i & -0.401986 + 1.468494i \\ 0.043442 + 0.592788i & 0.090347 + 0.771653i \\ 0.013536 + 0.360353i & 0.020075 + 0.430424i \\ 0.043442 + 0.592788i & 0.013536 + 0.360353i \\ 0.090347 + 0.771653i & 0.020075 + 0.430424i \\ 0.276110 + 1.677311i & -0.019449 + 0.549477i \\ -0.019449 + 0.549477i & -0.241045 + 0.959518i \end{pmatrix}.$$

With the second kind differentials

$$(30) \quad dr_{2i-1}^{[s]} = \frac{\mathcal{R}_{2i-1}(x) dx}{-2s \sqrt{\mathcal{P}(x)}}, \quad i = 1, 2, 3, 4,$$

$$\begin{aligned} \mathcal{R}_1 &= x^4, \\ \mathcal{R}_3 &= 3x^5 + (78 - 20i)x^4 + (217 - 288i)x^3, \\ \mathcal{R}_5 &= 5x^6 + (156 - 40i)x^5 + (651 - 864i)x^4 - (15170 - 1652i)x^3 \\ &\quad - (79138 - 82462i)x^2, \\ \mathcal{R}_7 &= 7x^7 + (234 - 60i)x^6 + (1085 - 1440i)x^5 - (30340 - 3304i)x^4 \\ &\quad - (237414 - 247386i)x^3 + (648116 + 911692i)x^2 \\ &\quad + (4126332 - 3930980i)x. \end{aligned}$$

second kind periods are computed:

$$\begin{aligned} \eta &\approx \begin{pmatrix} 22.428062 - 6.098673i & -8.281570 + 4.260894i \\ 280.811215 - 73.921437i & -233.173130 + 22.293105i \\ 910.855655 + 10.721526i & -2603.233939 - 813.570166i \\ 1224.707652 + 409.922637i & -7484.857429 - 1328.792554i \\ & -0.205360 - 0.177582i \quad -0.198185 - 0.006055i \\ & 5.630286 - 0.370818i \quad -32.028810 + 11.479858i \\ & 299.647570 + 719.376216i \quad 1242.433044 + 350.238889i \\ & 487.787097 + 8861.332415i \quad 6189.443173 - 7889.884228i \end{pmatrix}, \\ \eta' &\approx \begin{pmatrix} 13.855811 + 9.185567i & 1.880170 - 4.181065i \\ 150.913701 + 40.841618i & 64.433701 - 272.113911i \\ 420.612695 + 72.624802i & 1188.248232 - 1359.820959i \\ 504.296929 + 98.209496i & 3559.979547 - 2711.948811i \\ & 0.264151 - 1.540944i \quad 0.305811 - 1.421979i \\ & -26.525723 - 208.762530i \quad -27.152420 - 206.017i \\ & -1290.627353 - 496.867943i \quad -1470.266735 - 1061.435845i \\ & -9584.859568 + 9412.897457i \quad -2002.776466 + 2196.979511i \end{pmatrix}. \end{aligned}$$

and the symmetric matrix

$$\varkappa \approx \begin{pmatrix} -26.150273 + 5.226639i & -113.639362 + 91.745099i \\ -113.639362 + 91.745099i & 2527.918193 + 333.2000001i \\ 815.048336 + 59.142845i & 6691.213749 - 15142.962600i \\ 2796.548807 - 2715.208601i & -19805.451622 - 22245.716646i \\ & 815.048336 + 59.142845i \quad 2796.548807 - 2715.208601i \\ & 6691.213749 - 15142.962600i \quad -19805.451622 - 22245.716646i \\ & -501204.576087 - 151451.871496i \quad -1572965.591976 + 1699015.043174i \\ & -1572965.591976 + 1699015.043174i \quad -403196.119224 + 19865411.502694i \end{pmatrix}.$$

Numerical integration is performed with the `WorkingPrecision` of 18. Then the relations (26) are satisfied with an accuracy of 10^{-16} , and the symmetric property of τ with an accuracy of 10^{-15} . The symmetric property of \varkappa is accurate up to 10^{-8} , and the Legendre relation up to 10^{-14} .

Verification. An analog of the Bolza formulas on a genus 4 hyperelliptic curve, see [5, Eq. (40)], is given by

$$(31) \quad e_\iota = -\frac{\partial_{u_1, u_7}^2 \theta[\{\iota\}](\omega^{-1}u)}{\partial_{u_1, u_5}^2 \theta[\{\iota\}](\omega^{-1}u)} \Big|_{u=0}.$$

According to the construction of the basis, we have the following correspondence between characteristics and branch points:

$$\begin{aligned} e_1 &= -18 - 2\iota & [\varepsilon_1] &= \begin{pmatrix} 1 & 0 & 0 & 0 \\ 0 & 0 & 0 & 0 \end{pmatrix} & [\{1\}] &= \begin{pmatrix} 0 & 1 & 1 & 1 \\ 0 & 1 & 0 & 1 \end{pmatrix}, \\ e_2 &= -16 + 5\iota & [\varepsilon_2] &= \begin{pmatrix} 1 & 0 & 0 & 0 \\ 1 & 0 & 0 & 0 \end{pmatrix} & [\{2\}] &= \begin{pmatrix} 0 & 1 & 1 & 1 \\ 1 & 1 & 0 & 1 \end{pmatrix}, \\ e_3 &= -11 + 3\iota & [\varepsilon_3] &= \begin{pmatrix} 0 & 1 & 0 & 0 \\ 1 & 0 & 0 & 0 \end{pmatrix} & [\{3\}] &= \begin{pmatrix} 1 & 0 & 1 & 1 \\ 1 & 1 & 0 & 1 \end{pmatrix}, \\ e_4 &= -10 - \iota & [\varepsilon_4] &= \begin{pmatrix} 0 & 1 & 0 & 0 \\ 1 & 1 & 0 & 0 \end{pmatrix} & [\{4\}] &= \begin{pmatrix} 1 & 0 & 1 & 1 \\ 1 & 0 & 0 & 1 \end{pmatrix}, \\ e_5 &= -4 + 2\iota & [\varepsilon_5] &= \begin{pmatrix} 0 & 0 & 1 & 0 \\ 1 & 1 & 0 & 0 \end{pmatrix} & [\{5\}] &= \begin{pmatrix} 1 & 1 & 0 & 1 \\ 1 & 0 & 0 & 1 \end{pmatrix}, \\ e_6 &= -3 + 3\iota & [\varepsilon_6] &= \begin{pmatrix} 0 & 0 & 1 & 0 \\ 1 & 1 & 1 & 0 \end{pmatrix} & [\{6\}] &= \begin{pmatrix} 1 & 1 & 0 & 1 \\ 1 & 0 & 1 & 1 \end{pmatrix}, \\ e_7 &= 3 + 3\iota & [\varepsilon_7] &= \begin{pmatrix} 0 & 0 & 0 & 1 \\ 1 & 1 & 1 & 0 \end{pmatrix} & [\{7\}] &= \begin{pmatrix} 1 & 1 & 1 & 0 \\ 1 & 0 & 1 & 1 \end{pmatrix}, \\ e_8 &= 7 - 2\iota & [\varepsilon_8] &= \begin{pmatrix} 0 & 0 & 0 & 1 \\ 1 & 1 & 1 & 1 \end{pmatrix} & [\{8\}] &= \begin{pmatrix} 1 & 1 & 1 & 0 \\ 1 & 0 & 1 & 0 \end{pmatrix}, \\ e_9 &= 13 - \iota & [\varepsilon_9] &= \begin{pmatrix} 0 & 0 & 0 & 0 \\ 1 & 1 & 1 & 1 \end{pmatrix} & [\{9\}] &= \begin{pmatrix} 1 & 1 & 1 & 1 \\ 1 & 0 & 1 & 0 \end{pmatrix}, \end{aligned}$$

where $[\{\iota\}] = [\varepsilon_\iota] + [K]$, and

$$(32) \quad [K] = \sum_{i=1}^4 [\varepsilon_{2i}] = \begin{pmatrix} 1 & 1 & 1 & 1 \\ 0 & 1 & 0 & 1 \end{pmatrix}.$$

The zero matrix serves as the characteristic $[\varepsilon_0]$ of the branch point e_0 at infinity. The method of computing characteristics is adopted from [15].

The formulas (31) are satisfied with an accuracy of 10^{-14} .

Remark 2. Period matrices of the first kind obtained for the curve (29) with the help of `algcurves` differ from the presented results, as well as a different and much more tangled homology basis is chosen for computation. The period matrices obtained from `algcurves` satisfy the Bolza formulas for nine half-integer characteristics. The correspondence between characteristics and branch points is not clear from the homology basis chosen for computation. Although, by computing the Bolza formulas for all characteristics one can find out this correspondence.

3.8. Example 2: Real branch points. Consider briefly the case of a curve (20) with all real branch points:

$$-18, -15, -11, -5, 1, 2, 7, 12, 16,$$

which is defined by the equation

$$(33) \quad 0 = -y^2 + x^9 + 11x^8 - 514x^7 - 4602x^6 + 82441x^5 + 506395x^4 - 4495768x^3 - 11079084x^2 + 54907920x - 39916800.$$

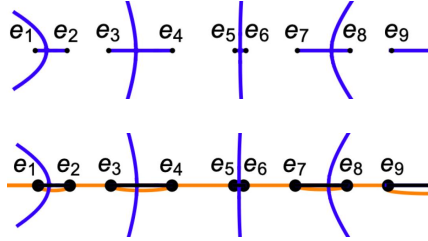


FIGURE 5. The contour Γ (blue), and a continuous path (orange).

The contour Γ and a continuous path through all branch points are shown on fig. 5. In this case, the sequence of signs has a clear pattern:

$$\{s_{0,1}, s_{1,2}, s_{2,3}, s_{3,4}, s_{4,5}, s_{5,6}, s_{6,7}, s_{7,8}, s_{8,9}, s_{9,0}\} = \{+1, -1, -1, +1, +1, -1, -1, +1, +1, -1\}.$$

Remark 3. Note, that cuts coincide with horizontal segments of the contour Γ , and so the sign changes when the left point of a cut is reached, that is at every e_{2k-1} , $k = 1, \dots, g+1$. This implies, $s_{4k-3,4k-2} = s_{4k-2,4k-1} = -1$, and $s_{4k-1,4k} = s_{4k,4k+1} = +1$, $k = 1, \dots$, since we always start with $s_{0,1} = +1$. The final segment has the sign $s_{2g+1,0} = -1$ if the genus is even, or $s_{2g+1,0} = +1$ if the genus is odd.

First kind not normalized periods are

$$\omega \approx \begin{pmatrix} -0.675637 & 0.287434 & 0.002651 & -0.309937 \\ 0.041299 & -0.032471 & 0.001599 & -0.031911 \\ -0.002535 & 0.003908 & 0.001010 & -0.003404 \\ 0.000156 & -0.000507 & 0.000673 & -0.000377 \end{pmatrix},$$

$$\omega' \approx \begin{pmatrix} -0.939638i & -0.289356i & -0.312311i & -0.394964i \\ 0.030634i & -0.018895i & -0.013110i & -0.028577i \\ -0.001371i & 0.002447i & 0.001224i & -0.002089i \\ 0.000066i & -0.000232i & 0.000698i & -0.000154i \end{pmatrix}.$$

Then the normalized period matrix from the Siegel upper half-space is

$$\tau \approx \begin{pmatrix} 1.602330i & 0.820786i & 0.514534i & 0.304355i \\ 0.820786i & 1.304404i & 0.648249i & 0.359593i \\ 0.514534i & 0.648249i & 1.686169i & 0.501628i \\ 0.304355i & 0.359593i & 0.501628i & 0.948644i \end{pmatrix}.$$

Remark 4. When all branch points are real, the path through all branch points coincides with the real axis. Moreover, $\mathcal{P}(x)$ is real-valued along the path, positive on segments $[e_{2k-1}, e_{2k}]$, $k = 1, \dots, g+1$, where cuts are made, and negative on the remaining segments $[e_{2k}, e_{2k+1}]$, $k = 0, \dots, g$. If one branch point is located at infinity, then e_0 stands for $-\infty$, and e_{2g+2} stands for ∞ . If all branch points are finite, then e_{2g+2} denotes the same point as e_0 , which is the smallest one.

Since $\mathcal{P}(x)$ has an alternating sign along the path, all \mathfrak{a} -periods are real, and all \mathfrak{b} -periods are purely imaginary. Moreover,

$$(34) \quad y(x) = (-i)^j \sqrt{|\mathcal{P}(x)|} \quad \text{on } [e_j, e_{j+1}], \quad j = 0, \dots, 2g+1.$$

The formula (34) was discovered by V. Enolsky. It shows how y_+ and y_- connect on Sheet a.

Second kind periods on (33) computed by (30) with

$$\begin{aligned}\mathcal{R}_1 &= x^4, \\ \mathcal{R}_3 &= 3x^5 + 22x^4 - 514x^3, \\ \mathcal{R}_5 &= 5x^6 + 44x^5 - 1542x^4 - 9204x^3 + 82441x^2, \\ \mathcal{R}_7 &= 7x^7 + 66x^6 - 2570x^5 - 18408x^4 \\ &\quad + 247323x^3 + 1012790x^2 - 4495768x.\end{aligned}$$

are

$$\begin{aligned}\eta &\approx \begin{pmatrix} 11.099150 & -2.673068 & 0.004562 & -3.109806 \\ 42.176466 & -129.207930 & -1.238236 & -5.426458 \\ -383.268207 & -1342.343715 & 100.817590 & 1906.755187 \\ -578.759149 & 4760.249993 & -2368.318297 & -1963.133866 \end{pmatrix}, \\ \eta' &\approx \begin{pmatrix} 3.501174i & -5.136174i & -5.034880i & -5.515607i \\ -11.2650450i & -187.532997i & -174.869192i & -151.780483i \\ -195.044640i & 288.885494i & 811.312906i & 816.306629i \\ -195.450172i & 1246.674997i & 6300.606235i & -562.511001i \end{pmatrix},\end{aligned}$$

and the symmetric matrix

$$\varkappa \approx \begin{pmatrix} -13.123159 & 129.285113 & 1107.820797 & -1910.386399 \\ 129.285113 & 1362.173530 & -26772.601447 & 34575.690532 \\ 1107.820797 & -26772.601447 & -519356.757226 & 988034.553637 \\ -1910.386399 & 34575.690532 & 988034.553637 & -5074619.889795 \end{pmatrix}.$$

Numerical integration is performed with the `WorkingPrecision` of 18. The same accuracy as in Example 1 is achieved.

4. COMPUTATION OF \wp -FUNCTIONS ON A HYPERELLIPTIC CURVE

In this section computation of \wp -functions on an arbitrary divisor is presented. First, the Abel image $\mathcal{A}(D)$ of a given divisor D is computed, then \wp -functions are calculated at $u = \mathcal{A}(D)$ by means of (12). The solution (15) of the Jacobi inversion problem is used for verification.

The characteristic $[K]$ of the vector of Riemann constants is required to define \wp -functions accurately. On a hyperelliptic curve, $[K]$ is computed as a sum of odd characteristics corresponding to branch points, cf. (32). The theta function with this characteristic has the maximal order of vanishing at $v = 0$, which corresponds to the Sato weight of the sigma function, which is $\text{wgt } \sigma = -\frac{1}{2}(g+1)g$.

Let $D = \sum_{i=1}^n P_i$ be a divisor on a curve. We suppose that D is non-special, that is $n \geq g$, and D does not contain pairs of points connected by the hyperelliptic involution. On special divisors σ -function vanishes, and so \wp -functions have singularities. The Abel image is computed by

$$(35) \quad \mathcal{A}(D) = \sum_{i=1}^n \mathcal{A}(P_i),$$

where the Abel image of a point is defined by (3), and the standard not normalized holomorphic differentials (23) are used. The Riemann surface constructed in the

previous section is used to draw paths to points of D . Below, an explanation how to choose such a path correctly is given.

Let $P_i = (x_i, y_i)$. We choose e_i in the vicinity of x_i , such that y_s does not change the sign over the segment $[e_i, x_i]$. The sheet where P_i is located is identified from comparing the sign n of $y_i = y_n(x_i)$ with the sign on $[e_i, x_i]$ according to the sequence of signs on Sheet a. A path to P_i is drawn on the sheet where the point is located. The path starts at $-\infty$ on the real axis, and goes to e_i along the continuous path chosen to construct the Riemann surface. Then the segment $[e_i, x_i]$ is added to this path. If the path to P_i is chosen correctly, then the final sign coincides with n , and so the point P_i is reached. Along the path to P_i the Abel image $\mathcal{A}(P_i)$ is computed.

The proposed algorithm is illustrated by examples. Divisors of degree equal to the genus g of a curve are considered, and so the Jacobi inversion problem is used for verification. One can compute \wp -functions on a divisor of degree greater than g , and solve the Jacobi inversion problem for the corresponding reduced divisor.

4.1. Example 1a. We continue to work with the curve (29) from Example 1 in the previous section.

Let u be the Abel map of a non-special divisor $D = \sum_{i=1}^4 P_i$,

$$\begin{aligned} P_1 &= (x_1, y_1) = (-9 + i, -8\sqrt{-918645 - 541515i}) \\ &\approx (-9 + i, -2174.219935 + 7969.975679i), \\ P_2 &= (x_2, y_2) = (-4 - 3i, -20\sqrt{924613 - 1261876i}) \\ &\approx (-4 - 3i, -22311.336861 + 11311.522997i), \\ P_3 &= (x_3, y_3) = (1 + 2i, 10\sqrt{-1744002 + 734019i}) \\ &\approx (1 + 2i, 2721.885087 + 13483.651524i), \\ P_4 &= (x_4, y_4) = (6 + 4i, -4\sqrt{99702405 - 110095815i}) \\ &\approx (6 + 4i, -44563.130818 + 19764.466810i). \end{aligned}$$

Actually, $y_i = y_+(x_i)$ for all i . Using the sequence of signs on Sheet a, and fig. 4,

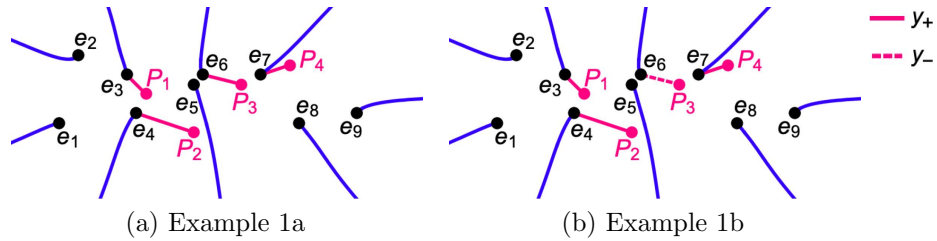


FIGURE 6. Paths to points of divisor D .

we find that P_1, P_2, P_4 are located on Sheet a, and P_3 is located on Sheet b. Then we compute the Abel images, see location of points P_i on fig. 6(a)

$$\mathcal{A}(P_1) = \mathcal{A}_{0,1}^{[+]} + \sum_{i=1}^2 \mathcal{A}_{i,i+1}^{[-]} + \int_{e_3}^{x_1} du^{[+]},$$

$$\begin{aligned}\mathcal{A}(P_2) &= \mathcal{A}_{0,1}^{[+]} + \sum_{i=1}^3 \mathcal{A}_{i,i+1}^{[-]} + \int_{e_4}^{x_2} du^{[+]}, \\ \mathcal{A}(P_3) &= -\left(\mathcal{A}_{0,1}^{[+]} + \sum_{i=1}^3 \mathcal{A}_{i,i+1}^{[-]} + \mathcal{A}_{4,5}^{[+]} + \mathcal{A}_{5,6}^{[-]} + \int_{e_6}^{x_3} du^{[-]}\right), \\ \mathcal{A}(P_4) &= \mathcal{A}_{0,1}^{[+]} + \sum_{i=1}^3 \mathcal{A}_{i,i+1}^{[-]} + \mathcal{A}_{4,5}^{[+]} + \sum_{i=5}^6 \mathcal{A}_{i,i+1}^{[-]} + \int_{e_7}^{x_4} du^{[+]},\end{aligned}$$

and find

$$u(D) = \sum_{i=1}^4 \mathcal{A}(P_i) \approx \begin{pmatrix} -1.182750 + 0.205635i \\ 0.073714 - 0.038375i \\ -0.004762 + 0.002674i \\ 0.000592 - 0.000064i \end{pmatrix}.$$

By means of (12) we obtain

$$\begin{aligned}(36) \quad \wp_{1,1}(u(D)) &\approx -6 + 4i, & \wp_{1,1,1}(u(D)) &\approx 91.581255 - 159.929002i, \\ \wp_{1,3}(u(D)) &\approx 42 + 53i, & \wp_{1,1,3}(u(D)) &\approx 23.849556 - 1665.831810i, \\ \wp_{1,5}(u(D)) &\approx 193 + 191i, & \wp_{1,1,5}(u(D)) &\approx -6971.970187 - 998.734510i, \\ \wp_{1,7}(u(D)) &\approx 446 - 578i, & \wp_{1,1,7}(u(D)) &\approx -5733.795768 - 18693.578334i.\end{aligned}$$

Next, we use the solution (15) of the Jacobi inversion problem to verify if the obtained Abel image corresponds to the given divisor D on the curve, and at the same time to verify the compliance of the obtained periods with the curve. On a hyperelliptic curve of genus 4 this solution acquires the form

$$\begin{aligned}\mathcal{R}_8(x; u) &\equiv x^4 - x^3 \wp_{1,1}(u) - x^2 \wp_{1,3}(u) - x \wp_{1,5}(u) - \wp_{1,7}(u) = 0, \\ \mathcal{R}_9(x, y; u) &\equiv 2y + x^3 \wp_{1,1,1}(u) + x^2 \wp_{1,1,3}(u) + x \wp_{1,1,5}(u) + \wp_{1,1,7}(u) = 0.\end{aligned}$$

The two entire rational functions in x and y , namely \mathcal{R}_8 and \mathcal{R}_9 , which both vanish on D , can be obtained as determinants of the two matrices, respectively,

$$\begin{aligned}\mathcal{R}_8(D) &= \begin{pmatrix} 1 & x & x^2 & x^3 & x^4 \\ \{1 & x_i & x_i^2 & x_i^3 & x_i^4\}_{i=1}^4 \end{pmatrix}, \\ \mathcal{R}_9(D) &= \begin{pmatrix} 1 & x & x^2 & x^3 & y \\ \{1 & x_i & x_i^2 & x_i^3 & y_i\}_{i=1}^4 \end{pmatrix}.\end{aligned}$$

After a proper normalization, we obtain

$$(37a) \quad \mathcal{R}_8(x; u(D)) = x^4 + (6 - 4i)x^3 - (42 + 53i)x^2 - (193 + 191i)x - 446 + 578i,$$

$$\begin{aligned}(37b) \quad \mathcal{R}_9(x, y; u(D)) &= 2y + (91.581255 - 159.929002i)x^3 \\ &+ (23.849556 - 1665.831810)x^2 - (6971.970187 + 998.734510i)x \\ &- 5733.795768 - 18693.578334i,\end{aligned}$$

Coefficients of \mathcal{R}_8 and \mathcal{R}_9 give values of \wp -functions on D , which coincide with (36) with an accuracy of 10^{-12} .

4.2. Example 1b. Let D from Example 1a be slightly modified, by moving P_3 on Sheet a, where $y_3 = y_-(x_3)$. That is

$$\begin{aligned} P_3 = (x_3, y_3) &= (1 - 2i, -10\sqrt{-1744002 + 734019i}) \\ &\approx (1 + 2i, -2721.885087 - 13483.651524i). \end{aligned}$$

Then $\mathcal{A}(P_3)$ is computed with the opposite sign:

$$\mathcal{A}(P_3) = \mathcal{A}_{0,1}^{[+]} + \sum_{i=1}^3 \mathcal{A}_{i,i+1}^{[-]} + \mathcal{A}_{4,5}^{[+]} + \mathcal{A}_{5,6}^{[-]} + \int_{e_6}^{x_3} du^{[-]}.$$

Thus,

$$u(D) = \sum_{i=1}^4 \mathcal{A}(P_i) \approx \begin{pmatrix} -1.574832 + 0.029543i \\ 0.073141 - 0.050092i \\ -0.003641 + 0.002439i \\ 0.000890 + 0.000121i \end{pmatrix}.$$

Values of $\wp_{1,2i-1}$, $i = 1, 2, 3, 4$, remain the same, within the accuracy. The new values of $\wp_{1,1,2i-1}$, are

$$\begin{aligned} \wp_{1,1,1}(u(D)) &\approx -51.390396 - 175.145987i, \\ \wp_{1,1,3}(u(D)) &\approx -1007.385975 - 1486.407403i, \\ \wp_{1,1,5}(u(D)) &\approx -3163.745380 + 5334.829741i, \\ \wp_{1,1,7}(u(D)) &\approx 10094.385116 + 25500.899104i. \end{aligned} \tag{38}$$

Evidently, \mathcal{R}_8 remains unchanged, since values of x_i are kept the same. The new function \mathcal{R}_9 acquires the form

$$\begin{aligned} \mathcal{R}_9(x, y; u(D)) &= 2y - (51.390396 + 175.145987i)x^3 \\ &\quad - (1007.385975 + 1486.407403i)x^2 - (3163.745380 - 5334.829741i)x \\ &\quad + 10094.385116 + 25500.899104i, \end{aligned}$$

and its coefficients coincide with the values (38) with an accuracy of 10^{-10} .

5. PERIODS ON A TRIGONAL CURVE

5.1. Trigonal curves. A generic trigonal curve is defined by the equation

$$0 = f(x, y) = -y^3 + y^2\mathcal{T}(x) + y\mathcal{Q}(x) + \mathcal{P}(x). \tag{39}$$

Let maximal degrees of polynomials \mathcal{P} , \mathcal{Q} , \mathcal{T} be as shown in the table below, then the genus g of a curve is computed as follows

- Case 1: $\deg \mathcal{P} = 3m + 1$, $\deg \mathcal{Q} = 2m$, $\deg \mathcal{T} = m$, $g = 3m$;
- Case 2: $\deg \mathcal{P} = 3m + 2$, $\deg \mathcal{Q} = 2m + 1$, $\deg \mathcal{T} = m$, $g = 3m + 1$;
- Case 3: $\deg \mathcal{P} = 3m + 3$, $\deg \mathcal{Q} = 2m + 2$, $\deg \mathcal{T} = m + 1$, $g = 3m + 1$.

Note, that $y^2\mathcal{T}(x)$ is eliminated by the map $y \mapsto \tilde{y} + \frac{1}{3}\mathcal{T}(x)$, which leads to

$$\begin{aligned} 0 &= f(x, \tilde{y}) = -\tilde{y}^3 + \tilde{\mathcal{Q}}(x)\tilde{y} + \tilde{\mathcal{P}}(x), \\ \tilde{\mathcal{Q}}(x) &= \mathcal{Q}(x) + \frac{1}{3}\mathcal{T}(x)^2, \\ \tilde{\mathcal{P}}(x) &= \mathcal{P}(x) + \frac{1}{3}\mathcal{Q}(x)\mathcal{T}(x) + \frac{2}{27}\mathcal{T}(x)^3. \end{aligned}$$

Then the discriminant of (39) is

$$(40) \quad \Delta(x) = \tilde{\mathcal{P}}(x)^2 - \frac{4}{27}\tilde{\mathcal{Q}}(x)^3.$$

where

$$(41) \quad \deg \Delta = \begin{cases} 6m + 2, & \text{Case 1;} \\ 6m + 4, & \text{Case 2;} \\ 6m + 6, & \text{Case 3.} \end{cases}$$

The degree of Δ shows the number of finite branch points $B_i = \{(e_i, h_i)\}$. In Case 3 a curve has $6m + 6$ branch points, all finite. In Cases 1 and 2 a curve has the indicated in (41) number of finite branch points, and a double branch point at infinity. Let ν_i be the ramification index of B_i . Each branch point is counted $\nu_i - 1$ times. We assume, that all finite branch points have the ramification index 2, and the branch point at infinity B_0 has $\nu_0 = 3$.

Cases 1 and 2 with $\mathcal{T}(x) \equiv 0$ represent (n, s) -curves, which serve as canonical forms of trigonal curves. In these cases, the genus is computed by the formula $g = \frac{1}{2}(n - 1)(s - 1)$, see [9]. Case 3 is obtained by a proper bi-rational transformation from Case 2, thus the both cases have the same Weierstrass gap sequence \mathfrak{W} . Therefore, classification of trigonal curves is based on Cases 1 and 2. The corresponding gap sequences are (each set is supposed to be ordered ascendingly)

$$\begin{aligned} \text{Case 1} \quad \mathfrak{W} &= \{3i - 2 \mid i = 1, \dots, m\} \cup \{3i - 1 \mid i = 1, \dots, 2m\}; \\ \text{Case 2} \quad \mathfrak{W} &= \{3i - 1 \mid i = 1, \dots, m\} \cup \{3i - 2 \mid i = 1, \dots, 2m + 1\}. \end{aligned}$$

With the help of Sato weights the order relation is introduced in the space of monomials $y^j x^i$. The latter are used to construct the equation of a curve, and also canonical differentials. The ordered lists of monomials in the both cases are

$$(42a) \quad \text{Case 1: } \mathfrak{M} = \{1, x, \dots, x^{m-1}, x^m, y, x^{m+1}, yx, \dots, x^{2m-1}, yx^{m-1}, x^{2m}, yx^m, y^2, x^{2m+1}, yx^{m+1}, \{y^2 x^i, x^{2m+1+i}, yx^{m+1+i} \mid i \in \mathbb{N}\}\},$$

$$(42b) \quad \text{Case 2: } \mathfrak{M} = \{1, x, \dots, x^{m-1}, x^m, y, x^{m+1}, yx, \dots, x^{2m-1}, yx^{m-1}, x^{2m}, yx^m, x^{2m+1}, y^2, yx^{m+1}, x^{2m+2}, \{y^2 x^i, yx^{m+1+i}, x^{2m+2+i} \mid i \in \mathbb{N}\}\}.$$

5.2. Riemann surface. In what follows, we focus on the canonical forms of trigonal curves

$$(43) \quad 0 = f(x, y) = -y^3 + y\mathcal{Q}(x) + \mathcal{P}(x).$$

with the discriminant polynomial

$$\Delta(x) = \mathcal{P}(x)^2 - \frac{4}{27}\mathcal{Q}(x)^3.$$

Suppose, that all roots of Δ are distinct, also \mathcal{P} and \mathcal{Q} have no common roots. These conditions are sufficient for the situation when the ramification index of every finite branch point is 2.

Solutions of (43) are given by the formula

$$(44a) \quad \begin{aligned} y_{+,a}(x) &= q_{+,a}(x) + \frac{1}{3}\mathcal{Q}(x)q_{+,a}^{-1}(x), \quad a = 1, 2, 3, \\ q_{+,a}(x) &= v_+^{1/3}(x)e^{2(a-1)\imath\pi/3}, \quad v_+(x) = \frac{1}{2}\left(\mathcal{P}(x) + \sqrt{\Delta(x)}\right), \end{aligned}$$

or equivalently

$$(44b) \quad y_{-,a}(x) = q_{-,a}(x) + \frac{1}{3}\mathcal{Q}(x)q_{-,a}^{-1}(x), \quad a = 1, 2, 3,$$

$$q_{-,a}(x) = v_{-}^{1/3}(x) e^{2(a-1)\imath\pi/3}, \quad v_{-}(x) = \frac{1}{2}(\mathcal{P}(x) - \sqrt{\Delta(x)}),$$

where $\sqrt{\Delta}$ is defined by (22). By $q_{s,a}$, $s = \pm 1$, $a = 1, 2, 3$, three cubic roots of v_s are denoted. Let

$$(45) \quad v_s^{1/3}(x) = \begin{cases} |v_s(x)|^{1/3} e^{(\imath/3) \arg v_s(x)} & \text{if } \arg v_s(x) \geq 0, \\ |v_s(x)|^{1/3} e^{(\imath/3) \arg v_s(x) + \imath 2\pi/3} & \text{if } \arg v_s(x) < 0. \end{cases}$$

According to this definition, the function $v_s^{1/3}$ has the range $[0, \frac{2}{3}\pi)$, and its discontinuity is located over the contour $\Upsilon_s = \{x \mid \arg v_s(x) = 0\}$.

Theorem 2. *Let $v_s^{1/3}$ be defined by (45). Then each $y_{s,a}$ defined by (44) has discontinuity over the contour $\Upsilon_s = \{x \mid \arg v_s(x) = 0\}$. Along a path from a region with $\arg v_s(x) < 0$ to a region with $\arg v_s(x) \geq 0$ the analytic continuation of $y_{s,a}$ is given by $y_{s,b}$, where $a \mapsto b$ according to the cyclic permutation (123).*

Proof. Let $s = +1$. Let \tilde{x} be located in the vicinity of the contour Υ_+ , more precisely $|\arg v_+(\tilde{x})| < 3\phi$, with a small positive value ϕ . Then $0 \leq \arg v_+^{1/3}(\tilde{x}) < \phi$ if $\arg v_+(\tilde{x}) \geq 0$, and $\frac{2}{3}\pi - \phi < \arg v_+^{1/3}(\tilde{x}) < \frac{2}{3}\pi$ if $\arg v_+(\tilde{x}) < 0$. Therefore, Υ_+ is the contour of discontinuity of $v_+^{1/3}$.

Now, we find how the three values $q_{+,a}$ of $v_+^{1/3}$ are connected over Υ_+ . Let $U(x_0; \delta)$ be a disc of radius δ with the center at $x_0 \in \Upsilon_+$. The contour Υ_+ divides the disc into two parts: U_+ where $\arg v_+(x) \geq 0$, and U_- where $\arg v_+(x) < 0$. The analytic continuation of $v_+^{1/3}(x) = q_{+,1}(x)$ from U_+ to U_- is given by $e^{-\frac{2}{3}\imath\pi} v_+^{1/3}(x) = q_{+,3}(x)$, since $-\phi < \arg q_{+,3}(x) < 0$ if $x \in U_-$, and so continuously connects to $q_{+,1}$ with the range $[0, \phi)$ on U_+ . Similarly, the analytic continuation of $v_+^{1/3}(x) = q_{+,1}(x)$ from U_- to U_+ is given by $e^{\frac{2}{3}\imath\pi} v_+^{1/3}(x) = q_2(x)$. Therefore, along a path from U_- to U_+ , the function q_1 continuously connects to q_2 , then q_2 connects to q_3 , and q_3 connects to q_1 .

The same is true for $s = -1$. □

Theorem 3. *Let $\sqrt{\Delta}$ be defined by (22). Then among three values of y , given by (44a), or (44b), two have discontinuity over the contour $\Gamma = \{x \mid \arg \Delta(x) = 0\}$. If Γ_i is a segment of Γ which starts at a branch point $B_i = (e_i, h_i)$, and $h_i = y_a(e_i) = y_b(e_i)$, then y_a, y_b are discontinuous over Γ_i , and y_a serves as the analytic continuation of y_b on the other side of Γ_i , and vice versa.*

Proof. According to Theorem 1, the both functions v_+, v_- , defined in (44), have discontinuity over the contour $\Gamma = \{x \mid \arg \Delta(x) = 0\}$, and serve as analytic continuations of each other. This implies that all $q_{s,a}$ have discontinuity over Γ , and for every a the analytic continuation of $q_{+,a}$ is given by $q_{-,a}$, and vice versa. We assume that $y_{+,a}$, $a = 1, 2, 3$, have discontinuity over Γ , which follows from the same property of $q_{+,a}$.

Recall the relation $v_+^{1/3}(x)v_-^{1/3}(x) = \frac{1}{3}e^{2n\imath\pi/3}\mathcal{Q}(x)$, where $n = 0, 1$, or 2 , such that $\arg v_+(x) + \arg v_-(x) = 3\arg \mathcal{Q}(x) + 2\pi n$ holds in the vicinity of x . This implies three equalities of the form $y_{+,a_1}(x) = y_{-,a_2}(x)$, where $a_1 \mapsto a_2$ according to one of the transpositions: (12), (13), or (23). Indeed,

$$\begin{aligned} n = 0 \quad & y_{+,1}(x) = y_{-,1}(x), \quad y_{+,2}(x) = y_{-,3}(x), \quad y_{+,3}(x) = y_{-,2}(x); \\ n = 1 \quad & y_{+,1}(x) = y_{-,3}(x), \quad y_{+,2}(x) = y_{-,2}(x), \quad y_{+,3}(x) = y_{-,1}(x); \\ n = 2 \quad & y_{+,1}(x) = y_{-,2}(x), \quad y_{+,2}(x) = y_{-,1}(x), \quad y_{+,3}(x) = y_{-,3}(x). \end{aligned}$$

Taking into account, that over Γ at every a the analytic continuation of $y_{+,a}$ is given by $y_{-,a}$, we see that among the three values of y given by (44a), or (44b), one remains continuous, and the other two serve as analytic continuations of each other. Indeed, let $n = 0$ in the vicinity of x , then $y_{+,1}(x) = y_{-,1}(x)$. On the other hand, if a segment of Γ is located in this vicinity of x , then $y_{-,1}$ serves as the analytic continuation of $y_{+,1}$ on the other side of the segment, and so $y_{+,1}$ remains continuous. At the same time, $y_{-,2}(x) = y_{+,3}(x)$ serves as the analytic continuation of $y_{+,2}(x) = y_{-,3}(x)$, as follows from Theorem 1.

The contour Γ consists of segments Γ_i , each starts at e_i such that $B_i = (e_i, h_i)$ is a branch point, and ends at infinity. Let $x_0 \in \Gamma_i$ be located in the vicinity of e_i which does not contain Υ_+ , and $h_i = y_{+,a}(e_i) = y_{+,b}(e_i)$. Let $U(x_0, \delta)$ be a disc of radius δ centered at x_0 , such that $|x_0 - e_i| \geq \delta$. Then $U(x_0, \delta)$ is divided by Γ_i into two parts: U_+ where $\arg \Delta(x) \geq 0$, and U_- where $\arg \Delta(x) < 0$. There exists such c that $y_{+,c}(x) = y_{-,c}(x)$ for every $x \in U(x_0, \delta)$, and so $y_{+,c}$ is continuous over $U(x_0, \delta)$. Then a, b are the other two values from $\{1, 2, 3\}$, since $y_{+,a}(x) = y_{-,b}(x)$ and $y_{+,b}(x) = y_{-,a}(x)$ over $U(x_0, \delta)$. Indeed, due to $\Delta(e_i) = 0$ we have $y_{+,a}(e_i) = y_{+,b}(e_i)$.

Similar considerations can be made in the case of $s = -1$. \square

In what follows, we work with solutions $y_{+,a}$, $a = 1, 2, 3$, computed by the formula (44a), and denote them by y_a .

5.3. Continuous path. In order to determine the Riemann surface, a continuous path through all branch points should be chosen. Based on the investigation presented in subsection 5.2, the following algorithm is suggested.

1. Find all finite branch points $\{B_i = (e_i, h_i)\}_{i=1}^N$, and sort ascendingly first by $\operatorname{Re} e_i$, then by $\operatorname{Im} e_i$. The points are enumerated according to this order. Each point B_i is labeled by ' $a-b$ ', such that $h_i = y_a(e_i) = y_b(e_i)$, which means that solutions y_a and y_b connect over the segment Γ_i , which goes from e_i to infinity.
2. According to the order, a path on the Riemann sphere through all e_i is constructed from straight line segments $[e_i, e_{i+1}]$, $i = 1, \dots, N$. Then the segment $(-\infty, e_1]$ is added at the beginning of the polygonal path, and $[e_N, \infty)$ at the end.
3. Plot the contour $\Gamma = \{x \mid \arg \Delta(x) = 0\}$, see blue contours on fig. 7, and the contour $\Upsilon_+ = \{x \mid \arg v_+(x) = 0\}$, see green contours on fig. 7. Identify a permutation which corresponds to each segment of Γ_i , and Υ_+ . When the path crosses Γ_i , solutions y_a and y_b interchange. When the path crosses Υ_+ , solutions y_a, y_b, y_c permute in the corresponding cycle.
4. Moving along the polygonal path from the left to the right, passing e_i and cuts from the below, counter-clockwise, and taking into account intersections with Γ and Υ_+ , find the sequence of changes of solutions y_a , $a = 1, 2, 3$, starting from 1, 2, and 3:

$$\begin{aligned} \text{Sheet a: } & \{a_{0,1} = 1\} \cup \{a_{i,i+1}\}_{i=1}^{N-1} \cup \{a_{N,0}\}, \\ \text{Sheet b: } & \{b_{0,1} = 2\} \cup \{b_{i,i+1}\}_{i=1}^{N-1} \cup \{b_{N,0}\}, \\ \text{Sheet c: } & \{c_{0,1} = 3\} \cup \{c_{i,i+1}\}_{i=1}^{N-1} \cup \{c_{N,0}\}. \end{aligned}$$

Index 0 stands for infinity. Each sequence determines a sheet of the Riemann surface. Rounding infinity counter-clockwise, the path can be closed on each sheet. The three paths are homotopic to zero.

5.4. Homology. Note, that $N = 2(g+1)$ on a canonical trigonal curve. Therefore, finite branch points split into $g+1$ pairs. Without loss of generality, g cuts are made between branch points in pairs B_{2i}, B_{2i+1} , $i = 1, \dots, g$. These cuts go through finite points, on two sheets connected by points in a pair. One more cut is made from B_1 to B_N through infinity.

Let \mathbf{a}_i encircle the cut $[B_{2i}, B_{2i+1}]$ counter-clockwise. Let \mathbf{b}_i emerge from the cut $B_1-\infty-B_N$, and enter the cut encircled by \mathbf{a}_i . In this way a canonical homology basis is obtained.

5.5. Cohomology. First kind differentials are constructed with the help of the first g monomials from the ordered list \mathfrak{M} , namely:

$$(46) \quad du_{\mathbf{w}_i} = \frac{\mathbf{m}_{g-i+1}(x, y) dx}{\partial_y f(x, y)}, \quad i = 1, \dots, g,$$

where \mathbf{m}_k is the k -th element of \mathfrak{M} , and $\mathbf{w}_i \in \mathfrak{W}$.

A second kind differential $dr_{\mathbf{w}_i}$, $\mathbf{w}_i \in \mathfrak{W}$, is constructed with the help of the first $g+i$ monomials from \mathfrak{M} . Namely

$$(47) \quad dr_{\mathbf{w}_i} = \left(\sum_{j=1}^{g+i} c_{i,j} \mathbf{m}_j(x, y) \right) \frac{dx}{\partial_y f(x, y)}, \quad i = 1, \dots, g.$$

The relation (10) defines the coefficients of monomials \mathbf{m}_{g+i} , $i > 1$. Coefficients of the remaining part of the sum in (47) are also essential. In the case of trigonal curves, the second kind differentials associated to the standard first kind differentials (46) are obtained in [11], by means of the Klein formula.

5.6. Computation of periods. Next, first kind integrals on each segment along the polygonal path are computed:

$$(48a) \quad \mathcal{A}_{i,i+1}^{[\mathbf{n}_i, i+1]} = \int_{B_i}^{B_{i+1}} du^{[\mathbf{n}_i, i+1]}, \quad i = 1, \dots, N-1,$$

$$(48b) \quad \mathcal{A}_{0,1}^{[\mathbf{n}_0, 1]} = \int_{-\infty}^{B_1} du^{[\mathbf{n}_0, 1]}, \quad \mathcal{A}_{N,0}^{[\mathbf{n}_N, 0]} = \int_{B_N}^{\infty} du^{[\mathbf{n}_N, 0]},$$

where $\mathbf{n} = \mathbf{a}$, \mathbf{b} , or \mathbf{c} , depending on the sheet. The integrand of $\mathcal{A}_{i,j}^{[\mathbf{n}_i, j]}$ is defined by (46) with $y = y_{\mathbf{n}_i, j}(x)$. A lift of the continuous path to each sheet, closed by a semi-circle around infinity, is homotopic to zero, an so relations hold

$$(49) \quad \mathcal{A}_{0,1}^{[\mathbf{n}_0, 1]} + \sum_{i=1}^{N-1} \mathcal{A}_{i,i+1}^{[\mathbf{n}_i, i+1]} + \mathcal{A}_{N,0}^{[\mathbf{n}_N, 0]} = 0, \quad \mathbf{n} = \mathbf{a}, \mathbf{b}, \mathbf{c},$$

which serve for verification.

With a chosen basis of canonical cycles, first kind period matrices ω , and ω' are computed by (4), and the normalized period matrix is obtained

$$\tau = \omega^{-1} \omega',$$

which is required to be symmetric with positive imaginary part.

With the same basis of canonical cycles, second kind period matrices η , and η' are computed by (9) with differentials (47), and the symmetric matrix \varkappa from the definition of the sigma function is obtained by

$$\varkappa = \eta \omega^{-1}.$$

First and second kind period matrices satisfy the Legendre relation (11).

5.7. Example 3: (3,4)-curve. Consider the simplest trigonal curve in its canonical form

$$(50) \quad 0 = f(x, y) = -y^3 + x^4 + \lambda_2 yx^2 + \lambda_5 yx + \lambda_6 x^2 + \lambda_8 y + \lambda_9 x + \lambda_{12}.$$

From $\Delta(x) = 0$ we find x -coordinates e_i of branch points $B_i = (e_i, h_i)$. Then using (44a), we find the corresponding values of y_a , $a = 1, 2, 3$, two of which a, b coincide and give h_i . So each branch point is labeled by ‘ $a-b$ ’, that indicates which solutions connect in the vicinity of this branch point.

A (3,4)-curve possesses the gap sequence $\mathfrak{W} = \{1, 2, 5\}$, and the first kind differentials have the form

$$du = \begin{pmatrix} u_1 \\ u_2 \\ u_5 \end{pmatrix} = \begin{pmatrix} y \\ x \\ 1 \end{pmatrix} \frac{dx}{-3y^2 + \mathcal{Q}(x)}.$$

Let $\mathcal{A}_{i,j}^{[a]}$ denote the first kind integral between branch points B_i and B_j computed with solution $y = y_a(x)$:

$$(51) \quad \mathcal{A}_{i,j}^{[a]} = \int_{B_i}^{B_j} du^{[a]}.$$

Second kind differentials associated with the first ones on the curve (50) are defined as follows

$$dr = \begin{pmatrix} r_1 \\ r_2 \\ r_5 \end{pmatrix} = \begin{pmatrix} x^2 \\ 2xy \\ \mathcal{R}_5 \end{pmatrix} \frac{dx}{-3y^2 + \mathcal{Q}(x)},$$

$$\mathcal{R}_5 = 5x^2y + 3\lambda_3xy + \frac{2}{3}\lambda_2^2x^2 + \lambda_6y + \frac{2}{3}\lambda_2\lambda_5x.$$

Second kind integral $\mathcal{B}_{i,j}^{[a]}$ between B_i and B_j with solution $y = y_a(x)$ is computed by

$$(52) \quad \mathcal{B}_{i,j}^{[a]} = \int_{B_i}^{B_j} dr^{[a]}.$$

As an example, we consider a curve defined by the equation

$$(53) \quad 0 = f(x, y) \equiv -y^3 + x^4 + y(4x^2 + 5x + 11) + 3x^3 + 7x^2 + 16x + 9.$$

The curve has eight finite branch points:

$$\begin{array}{lll} e_1 \approx -4.58931, & h_1 \approx -4.9092 & 2-3 \\ e_2 \approx -1.17922 - 0.934455i, & h_2 \approx 1.60505 + 0.430221i & 1-3 \\ e_3 \approx -1.17922 + 0.934455i, & h_3 \approx 1.60505 - 0.430221i & 1-3 \\ e_4 \approx -0.431732 - 2.20256i, & h_4 \approx 0.309255 - 1.83532i & 2-3 \\ e_5 \approx -0.431732 + 2.20256i, & h_5 \approx 0.309255 + 1.83532i & 1-2 \\ e_6 \approx 0.499118 - 1.57527i, & h_6 \approx -1.80047 + 1.31135i & 1-2 \end{array}$$

$$\begin{aligned} e_7 &\approx 0.499118 + 1.57527i, & h_7 &\approx -1.80047 - 1.31135i & 2-3 \\ e_8 &\approx 0.812986, & h_8 &\approx -2.42959 & 2-3 \end{aligned}$$

In the right column the corresponding pair ‘ $a-b$ ’ is indicated.

Fig. 7(a) displays positions of e_i , and the contours where solutions y_a , $a = 1, 2, 3$, have discontinuity. The contour $\Upsilon_+ = \{x \mid \arg v_+(x) = 0\}$ is marked in green. Over

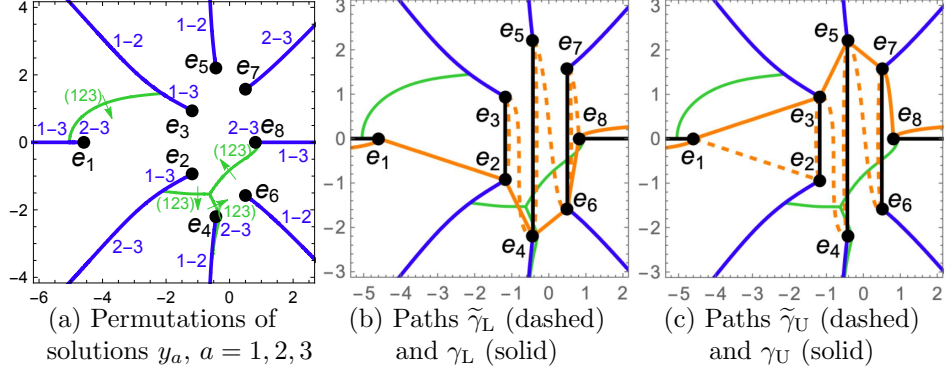


FIGURE 7. Contours Γ (blue), Υ_+ (green), cuts (black), and a path (orange).

Υ_+ all three solutions connect in pairs. Each segment of Υ_+ is labeled by the cyclic permutation (123) of the solutions, and an arrow shows in which direction this permutation occurs.

The contour $\Gamma = \{x \mid \arg \Delta(x) = 0\}$ is marked in blue. Each segment Γ_i of Γ starts at e_i and ends at infinity. Let $h_i = y_a(e_i) = y_b(e_i)$, then Γ_i is labeled by ‘ $a-b$ ’ in the vicinity of e_i . If Υ_+ intersects Γ_i at point d_i , then the segment of Γ_i between d_i and infinity is labeled by ‘ $b-c$ ’ such that $y_b(x) = y_c(x)$ for all x on this segment. Fig. 7(a) is in accordance with the density plots of $\arg y_a$, $a = 1, 2, 3$, shown on fig. 8.

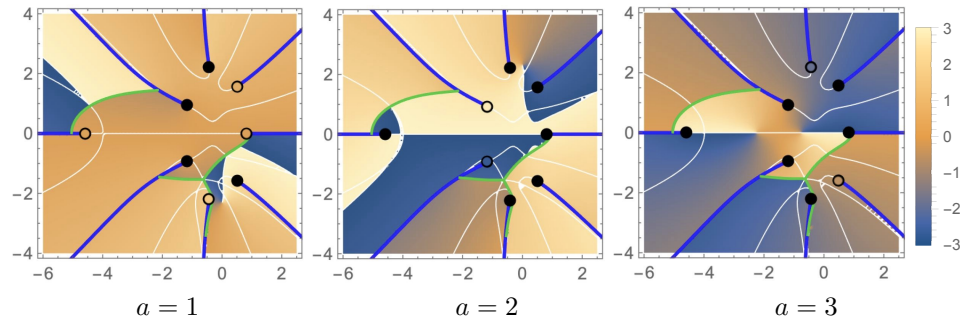


FIGURE 8. Density plot of $\arg y_a$, contours Γ (blue), Υ_+ (green).

Cuts connect pairs of points: B_2 to B_3 on sheets with solutions y_1 and y_3 , B_4 to B_5 on sheets with solutions y_1 and y_2 in the vicinity of B_5 which change consequently into the pair 1-3 and then 2-3 when approaching B_4 , and B_6 to B_7 on sheets with solutions y_2 and y_3 in the vicinity of B_7 which change into the pair 1-2 when approaching B_6 . One more cut goes from B_8 to infinity, and then to B_1 .

In the vicinity of B_8 solutions y_2 and y_3 connect, which change into the pair 1–3 in the vicinity of infinity, and then into 2–3 in the vicinity of B_1 .

Let a path $\tilde{\gamma}_L$ through all branch points be

$$(-\infty, e_1] \cup [e_1, e_2] \cup [e_2, e_3] \cup [e_3, e_4] \cup [e_4, e_5] \\ \cup [e_5, e_6] \cup [e_6, e_7] \cup [e_7, e_8] \cup [e_8, \infty),$$

as shown on fig. 7(b) in orange. The path is polygonal, and goes below points e_i and cuts, and so rounds cuts counter-clockwise. The path $\tilde{\gamma}_L$ is marked by dashed lines between e_2 and e_8 , and continuously deformed into a simpler path γ_L , which is marked by solid lines, and goes below points e_2, e_4, e_6 .

On fig. 7(c) an alternative path $\tilde{\gamma}_U$ through all branch points is presented, marked by dashed lines between e_1 and e_7 . The path $\tilde{\gamma}_U$ goes from the right to the left above points e_i and cuts, so the latter are rounded counter-clockwise. $\tilde{\gamma}_U$ is continuously deformed into a simpler path γ_U , which is marked by solid lines, and goes above points e_3, e_5, e_7 .

In what follows we work with the path $\tilde{\gamma}_L$, which mark sheets as follows

$$(54) \quad \begin{aligned} \{a_{0-1}, a_{1,2}, a_{2,3}, a_{3,4}, a_{4,5}, a_{5,6}, a_{6,7}, a_{7,8}, a_{8,0+}\} = \\ \text{Sheet a: } \{1, 1, 3, 3-1, 1-2-3, 3-2, 1-2, 2, 3\}, \\ \{b_{0-1}, b_{1,2}, b_{2,3}, b_{3,4}, b_{4,5}, b_{5,6}, b_{6,7}, b_{7,8}, b_{8,0+}\} = \\ \text{Sheet b: } \{2, 2, 2, 2-3, 2-3-1, 1-3, 3-1, 1, 1\}, \\ \{c_{0-1}, c_{1,2}, c_{2,3}, c_{3,4}, c_{4,5}, c_{5,6}, c_{6,7}, c_{7,8}, c_{8,0+}\} = \\ \text{Sheet c: } \{3, 3, 1, 1-2, 3-1-2, 2-1, 2-3, 3, 2\}. \end{aligned}$$

Connection of solutions y_1, y_2, y_3 on each sheet is shown on fig. 9.

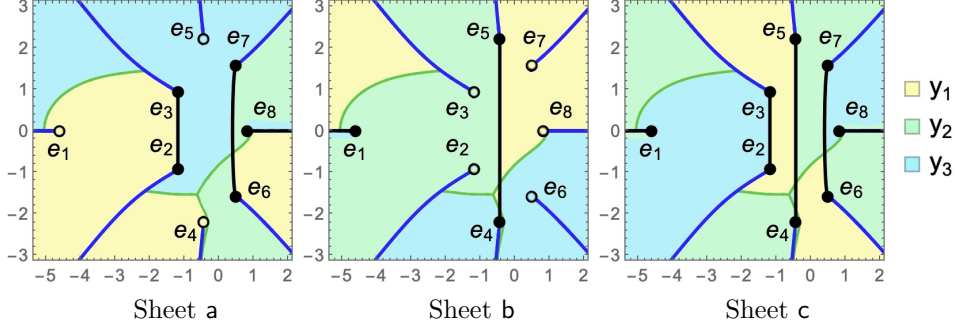


FIGURE 9. Connection of solutions y_1, y_2, y_3 on each sheet.

One can see that the cuts between B_2, B_3 , and between B_6, B_7 connect Sheets a and c, and the cut between B_4, B_5 connects Sheets b and c. The cut $B_8-\infty-B_1$ connects Sheets a and c on segment $[e_8, \infty)$, and Sheets b and c on $(\infty, e_1]$.

One can round infinity clockwise when moving along path γ_L from the left to the right and then along path γ_U from the right to the left. This is a circle around infinity on the Riemann sphere. Now we lift this circle to the curve.

Let start path γ_L^c at B_1 on Sheet c, and reach B_8 . The analytic continuation of y_3 is y_2 on the other side of Γ_8 in the vicinity of e_8 , and so we enter the cut and emerge on Sheet a, where segment $[e_8, \infty + i\epsilon]$ is governed by y_2 . Here we start path γ_U^a on Sheet a, and reach the point $(e_1, y_1(e_1))$, which is not a branch point. Thus, one full turn around infinity, denoted by γ_∞^{c-a} , is completed. We continue to move

along path γ_L^a on Sheet **a**, and reach B_8 . Solution y_2 connects to y_3 on the other side of Γ_8 in the vicinity of e_8 . So, we move from Sheet **a** to Sheet **c**, where segment $[e_8, \infty + i\epsilon]$ is governed by y_3 . Then we go along path γ_U^c on Sheet **c** and reach B_1 . At this point the second turn around infinity, denoted by γ_∞^{a-c} , is completed. In the vicinity of e_1 solution y_3 on Sheet **c** connects to y_2 on Sheet **b**. So we enter the cut and emerge on Sheet **b**, then move along path γ_L^b on Sheet **b**, and reach the point $(e_8, y_1(e_8))$. We continue to move along path γ_U^b on Sheet **b**, and reach B_1 . The third turn around infinity, denoted γ_∞^{b-b} , is completed by arrival to the initial point. This path around infinity $\gamma_{3\infty} \equiv \gamma_\infty^{c-a} \cup \gamma_\infty^{a-c} \cup \gamma_\infty^{b-b}$ can be used to reach an arbitrary point on the curve.

In fact, $a_{8,0+}$, $b_{8,0+}$, $c_{8,0+}$ in the sequences (54) do not belong to the sheets where they are listed. But the indicated paths, closed by a counter-clockwise semi-circle around infinity on each sheet, are homotopic to zero. Correspondingly, the sum of first kind integrals along each path vanishes. Along path γ_L the following relations are obtained

$$(55) \quad \begin{aligned} \mathcal{A}_{0-,1}^{[1]} + \mathcal{A}_{1,2}^{[1]} + \mathcal{A}_{2,4}^{[3-1]} + \mathcal{A}_{4,6}^{[1-2]} + \mathcal{A}_{6,8}^{[1-2]} + \mathcal{A}_{8,0+}^{[3]} &= 0, \\ \mathcal{A}_{0-,1}^{[2]} + \mathcal{A}_{1,2}^{[2]} + \mathcal{A}_{2,4}^{[2-3]} + \mathcal{A}_{4,6}^{[2-3]} + \mathcal{A}_{6,8}^{[3-1]} + \mathcal{A}_{8,0+}^{[1]} &= 0, \\ \mathcal{A}_{0-,1}^{[3]} + \mathcal{A}_{1,2}^{[3]} + \mathcal{A}_{2,4}^{[1-2]} + \mathcal{A}_{4,6}^{[3-1]} + \mathcal{A}_{6,8}^{[2-3]} + \mathcal{A}_{8,0+}^{[2]} &= 0, \end{aligned}$$

where $0-$ ($0+$) stands for $-\infty - i\epsilon$ ($\infty + i\epsilon$) and the superscript of $\mathcal{A}_{i,j}^{[a-b]}$ indicates that over the segment $[e_i, e_j]$ solution y_a changes into y_b . Note, the last relation follows from the first two, due to $\mathcal{A}_{i,j}^{[a_{i,j}]} + \mathcal{A}_{i,j}^{[b_{i,j}]} + \mathcal{A}_{i,j}^{[c_{i,j}]} = 0$, where $a_{i,j}$, $b_{i,j}$, and $c_{i,j}$ are three superscripts on Sheets **a**, **b**, and **c**, correspondingly.

Let path γ_U , starting from $\infty + i\epsilon$ and ending in $-\infty - i\epsilon$, be closed by a counter-clockwise semi-circle around infinity. On each sheet this path is homotopic to zero, and so produces another set of relations:

$$(56) \quad \begin{aligned} \mathcal{A}_{0+,8}^{[3]} + \mathcal{A}_{8,7}^{[2]} + \mathcal{A}_{7,5}^{[3]} + \mathcal{A}_{5,3}^{[3]} + \mathcal{A}_{3,1}^{[1]} + \mathcal{A}_{1,0-}^{[1]} &= 0, \\ \mathcal{A}_{0+,8}^{[2]} + \mathcal{A}_{8,7}^{[3]} + \mathcal{A}_{7,5}^{[2]} + \mathcal{A}_{5,3}^{[1]} + \mathcal{A}_{1,3}^{[3]} + \mathcal{A}_{1,0-}^{[2]} &= 0, \\ \mathcal{A}_{0+,8}^{[1]} + \mathcal{A}_{8,7}^{[1]} + \mathcal{A}_{7,5}^{[1]} + \mathcal{A}_{5,3}^{[2]} + \mathcal{A}_{3,1}^{[2]} + \mathcal{A}_{1,0-}^{[3]} &= 0. \end{aligned}$$

Note, that all branch points can be reached on Sheet **c**, as well as all cuts. Let a -cycles be located on Sheet **c**, encircling the three finite cuts. Let b_i -cycle emerge from the cut $B_8-\infty-B_1$, and enter the cut encircled by a_i -cycle, see fig. 10. Therefore, b_1 goes through Sheets **c** and **a**, b_2 through Sheets **c** and **b**, b_3 through Sheets **c** and **a**. Periods are calculated as follows

$$\begin{aligned} \omega_1 &= \mathcal{A}_{2,3}^{[1]} + \mathcal{A}_{3,2}^{[3]}, \\ \omega_2 &= \mathcal{A}_{4,5}^{[3-1-2]} + \mathcal{A}_{5,4}^{[1-3-2]} = \mathcal{A}_{4,6}^{[3-1]} + \mathcal{A}_{6,5}^{[1-2]} + \mathcal{A}_{5,2}^{[1]} + \mathcal{A}_{2,4}^{[1-2]}, \\ \omega_3 &= \mathcal{A}_{6,7}^{[2-3]} + \mathcal{A}_{7,6}^{[2-1]}, \\ \omega'_1 &= \mathcal{A}_{8,7}^{[3]} + \mathcal{A}_{7,5}^{[2]} + \mathcal{A}_{5,3}^{[1]} + \mathcal{A}_{3,6}^{[3-2]} + \mathcal{A}_{6,8}^{[1-2]}, \\ \omega'_2 &= \mathcal{A}_{1,2}^{[3]} + \mathcal{A}_{2,4}^{[1-2]} + \mathcal{A}_{4,2}^{[3-2]} + \mathcal{A}_{2,1}^{[2]}, \\ \omega'_3 &= \mathcal{A}_{8,7}^{[3]} + \mathcal{A}_{7,8}^{[2]}. \end{aligned}$$

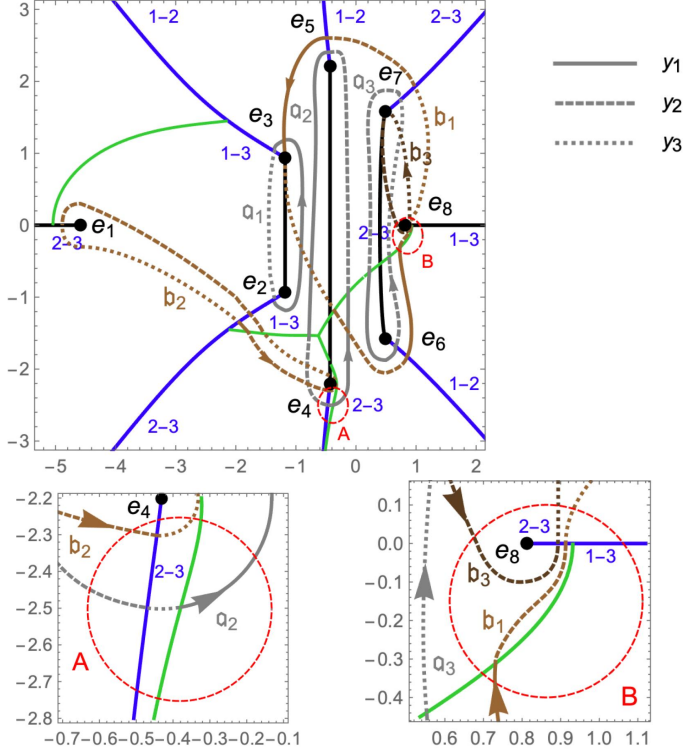


FIGURE 10. Canonical homology basis.

Computation gives the following not normalized period matrices

$$\omega \approx \begin{pmatrix} -0.646716i & 1.367235i & -1.406214i \\ 0.557691i & 0.662524i & 0.237700i \\ -0.425220i & -0.085658i & 0.761823i \end{pmatrix},$$

$$\omega' \approx \begin{pmatrix} 1.114221 + 0.360259i & -0.838244 + 0.360259i & 0.830310 - 0.703107i \\ -0.888801 + 0.610108i & -0.725076 + 0.610108i & -0.483530 + 0.118850i \\ 0.212490 - 0.255439i & 0.017209 - 0.255439i & -0.244951 + 0.380911i \end{pmatrix},$$

and the normalized period matrix from the Siegel upper half-space

$$\tau \approx \begin{pmatrix} 0.5 + 1.204054i & 0.5 + 0.179707i & 0.413339i \\ 0.5 + 0.179707i & 0.5 + 0.879769i & 0.176635i \\ 0.413339i & 0.176635i & 0.5 + 0.572103i \end{pmatrix}.$$

Second kind period matrices are

$$\eta \approx \begin{pmatrix} -0.541959i & -0.385425i & -0.722057i \\ 1.52536i & -0.88414i & 0.484784i \\ 0.975636i & -1.01088i & -2.65892i \end{pmatrix},$$

$$\eta' \approx \begin{pmatrix} -1.357307 - 0.463692i & 2.945439 - 0.463692i & -0.354124 - 0.361028i \\ 2.292766 + 0.320609i & 5.356432 + 0.320609i & 2.131611 + 0.242392i \\ -5.584050 - 0.017623i & 4.038588 - 0.017623i & 6.689080 - 1.329459i \end{pmatrix},$$

and the symmetric matrix

$$\varkappa \approx \begin{pmatrix} 0.180731 & -0.994032 & -0.304044 \\ -0.994032 & 0.540116 & -1.367017 \\ -0.304044 & -1.367017 & -3.624898 \end{pmatrix}.$$

All computations are done in Wolfram Mathematica 12, by means of the function `NIntegrate`. With the `WorkingPrecision` of 18, the relations (55) hold with an accuracy of 10^{-15} , as well as the symmetric property of τ . The symmetric property of \varkappa is satisfied up to 13 decimal digits.

6. COMPUTATION OF \wp -FUNCTIONS ON A TRIGONAL CURVE

Similar to the hyperelliptic case, the Abel image $\mathcal{A}(D)$ of a given divisor D is computed directly by the formula (35), then \wp -functions are calculated at $u = \mathcal{A}(D)$ by means of (12). The solution (16) or (17) of the Jacobi inversion problem is used for verification.

The accurate definition of \wp -functions requires the characteristic $[K]$ of the vector of Riemann constants K . This characteristic is half-integer, due to the relation $2K \sim \bar{\mathcal{A}}(C)$, which means that $2K$ is congruent to the Abel image of the canonical divisor C on the curve, and the latter is congruent to zero. Recall, that $\bar{\mathcal{A}}$ denotes the Abel map computed with normalized differentials. Moreover,

Proposition 1. *The theta function with characteristic $[K]$ possesses the maximal order of vanishing at $v = 0$, which is $(3m+2)m$ on a $(3, 3m+1)$ -curve, and $(3m+4)m$ on a $(3, 3m+2)$ -curve,*

Proof. Since the sigma function is defined through the theta function with characteristic $[K]$, cf. (8), the two functions have the same order of vanishing at the origin on the Jaconian variety. The order of vanishing of $\sigma(0)$ is shown by the Sato weight (with the opposite sign), which is given by the formula $\text{wgt } \sigma = -(n^2-1)(s^2-1)/24$, see [9]. By direct computations, one can find, that $\text{wgt } \sigma = (3m+2)m$ on a $(3, 3m+1)$ -curve, and $\text{wgt } \sigma = (3m+4)m$ on a $(3, 3m+2)$ -curve. \square

From the relation $[K] = [\frac{1}{2}\bar{\mathcal{A}}(C)]$ the location of the base point for computation can be found. In general, the base point is located at infinity. But it makes difference in computation on which sheet paths to points start.

Let $D = \sum_{i=1}^n P_i$ be a positive non-special divisor on a trigonal curve, which means: $\deg D = n \geq g$, and D does not contain any three points connected by involution on the curve. The Abel image of each point P_i is computed with the standard not normalized holomorphic differentials (46). A path to P_i is constructed as explain below.

Let $P_i = (x_i, y_i)$, $y_i = y_a(x_i)$, and from a the Sheet n where P_i is located can be identified. Let $Q_i = (e_i, y_a(e_i))$, where e_i is the x -coordinate of a branch point B_i , be in the vicinity to P_i on the same Sheet n . A path to P_i starts at $-\infty - i\epsilon$ on the fixed sheet, and goes to Q_i on Sheet n . Then the segment $[Q_i, P_i]$ on Sheet n is added to this path. Along the path to P_i the Abel image $\mathcal{A}(P_i)$ is computed.

Below, computation of \wp -functions is illustrated by examples. We consider divisors of degree equal to the genus g of the curve, and the Jacobi inversion problem is used for verification. The entire rational functions \mathcal{R}_{2g} and \mathcal{R}_{2g+1} , which give the solution (16), or (17), on a trigonal curve are obtained from a given divisor directly. Then coefficients are compared with ones obtained from the computed \wp -functions.

6.1. Example 3a. On the curve (50), with the homology basis chosen as shown on fig. 10, the vector of Riemann constants has the characteristic

$$(57) \quad [K] = \begin{pmatrix} 1 & 0 & 1 \\ 0 & 1 & 1 \end{pmatrix},$$

and $\theta[K]$ vanishes to the order 5 at $v = 0$.

This result corresponds to computation of the canonical divisor when paths to all branch points are located on Sheet c. That is, all paths start at $-\infty - \imath\epsilon$ on Sheet c, and go in the shortest way to branch points, all of which are located on Sheet c:

$$\begin{aligned} \omega \bar{\mathcal{A}}(C) = & \mathcal{A}_{0-,1}^{[3]} + (\mathcal{A}_{0-,1}^{[3]} + \mathcal{A}_{1,2}^{[3]}) + (\mathcal{A}_{0-,1}^{[3]} + \mathcal{A}_{1,2}^{[3]} + \mathcal{A}_{2,3}^{[1]}) \\ & + (\mathcal{A}_{0-,1}^{[3]} + \mathcal{A}_{1,2}^{[3]} + \mathcal{A}_{2,4}^{[1-2]}) + (\mathcal{A}_{0-,1}^{[3]} + \mathcal{A}_{1,2}^{[3]} + \mathcal{A}_{2,4}^{[1-2]} + \mathcal{A}_{4,6}^{[3-1]} + \mathcal{A}_{6,5}^{[1-2]}) \\ & + (\mathcal{A}_{0-,1}^{[3]} + \mathcal{A}_{1,2}^{[3]} + \mathcal{A}_{2,4}^{[1-2]} + \mathcal{A}_{4,6}^{[3-1]}) + (\mathcal{A}_{0-,1}^{[3]} + \mathcal{A}_{1,2}^{[3]} + \mathcal{A}_{2,4}^{[1-2]} + \mathcal{A}_{4,6}^{[3-1]} + \mathcal{A}_{6,7}^{[2-3]}) \\ & + (\mathcal{A}_{0-,1}^{[3]} + \mathcal{A}_{1,2}^{[3]} + \mathcal{A}_{2,4}^{[1-2]} + \mathcal{A}_{4,6}^{[3-1]} + \mathcal{A}_{6,8}^{[2-3]}) \approx \begin{pmatrix} 3.5 + 1.976806\imath \\ -1.5 + 2.115880\imath \\ 1.5 + 1.338712\imath \end{pmatrix}. \end{aligned}$$

The obtained vector of Riemann constants has components

$$(\bar{\mathcal{A}}(C))_j = \tau_{j,1} + 2\tau_{j,2} + \tau_{j,3} + 2\delta_{j,1} - 3\delta_{j,2} + \delta_{j,3},$$

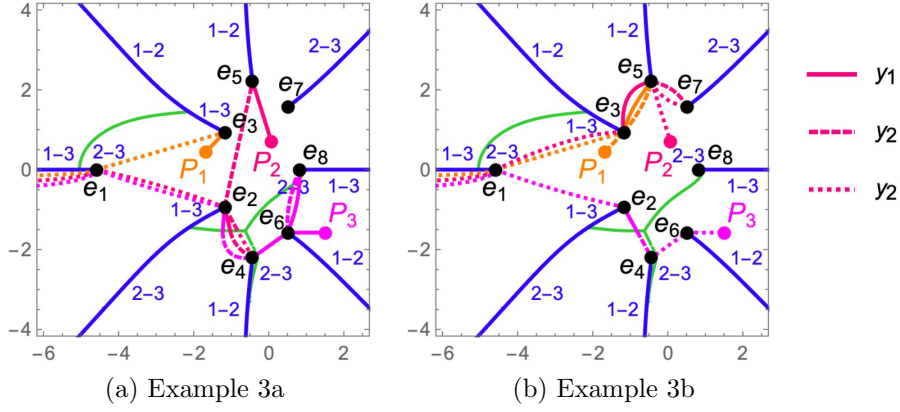
where $\delta_{i,j}$ denotes the Kronecker delta. This result coincides with (57).

Let a divisor be $D = \sum_{i=1}^3 P_i$ with

$$\begin{aligned} P_1 &= (e_3 - 0.5 - 0.5\imath, y_1(e_3 - 0.5 - 0.5\imath)) \\ &\approx (-1.679223 + 0.434455\imath, 3.431176 - 0.582699\imath), \\ P_2 &= (e_5 + 0.5 - 1.5\imath, y_1(e_5 + 0.5 - 1.5\imath)) \\ &\approx (0.068268 + 0.702564\imath, 3.555003 + 0.889027\imath), \\ P_3 &= (e_6 + 1, y_1(e_6 + 1)) \\ &\approx (1.499118 - 1.575269\imath, -4.191263 + 1.058317\imath). \end{aligned}$$

The points P_1 and P_3 are located on Sheet a, and P_2 on Sheet b. A path to each point starts at $-\infty - \imath\epsilon$ on Sheet c. Unlike the hyperelliptic case, a path to a point can not be started on any sheet, but on the fixed one, which is Sheet c in this example. Let P_1 on Sheet a be reached through the cut between B_2 and B_3 , then P_2 on Sheet b through the cut between B_4 and B_5 , and P_3 on Sheet a through the cut $B_8-\infty-B_1$, see fig. 11(a). Actually,

$$\begin{aligned} \mathcal{A}(P_1) &= \mathcal{A}_{0-,1}^{[3]} + \mathcal{A}_{1,3}^{[3]} + \int_{B_3}^{P_1} du^{[1]}, \\ \mathcal{A}(P_2) &= \mathcal{A}_{0-,1}^{[3]} + \mathcal{A}_{1,2}^{[3]} + \mathcal{A}_{2,4}^{[1-2]} + \mathcal{A}_{4,2}^{[3-2]} + \mathcal{A}_{2,5}^{[2]} + \int_{B_5}^{P_2} du^{[1]}, \\ \mathcal{A}(P_3) &= \mathcal{A}_{0-,1}^{[3]} + \mathcal{A}_{1,2}^{[3]} + \mathcal{A}_{2,4}^{[1-2]} + \mathcal{A}_{4,6}^{[3-1]} + \mathcal{A}_{6,8}^{[2-3]} + \mathcal{A}_{8,6}^{[2-1]} + \int_{B_6}^{P_3} du^{[1]}, \end{aligned}$$

FIGURE 11. Paths to points of divisor D .

where $du^{[a]}$ means that $y = y_a(x)$. The Abel image of D is

$$(58) \quad u(D) = \sum_{i=1}^3 \mathcal{A}(P_i) \approx \begin{pmatrix} -0.270333 - 1.612257i \\ -1.116879 + 0.562199i \\ 0.258194 + 0.268653i \end{pmatrix}.$$

By means of (12) we compute

$$(59) \quad \begin{aligned} \wp_{1,1}(u(D)) &\approx 0.059654 + 1.020925i, \\ \wp_{1,2}(u(D)) &\approx -0.793416 + 0.889005i, \\ \wp_{1,5}(u(D)) &\approx 0.885372 - 3.089764i, \\ \wp_{2,2}(u(D)) &\approx -0.269700 + 1.472739i, \\ \wp_{2,5}(u(D)) &\approx -3.501466 + 10.538856i, \\ \wp_{1,1,1}(u(D)) &\approx -2.156576 + 3.543516i, \\ \wp_{1,1,2}(u(D)) &\approx -3.595029 + 2.840859i, \\ \wp_{1,1,5}(u(D)) &\approx 5.656516 - 0.559812i. \end{aligned}$$

Alternatively, a part of the path $\gamma_{3\infty}$ around infinity can be used to reach each point. Denote

$$\begin{aligned} \mathcal{A}(\gamma_L^c) &= \mathcal{A}_{1,2}^{[3]} + \mathcal{A}_{2,4}^{[1-2]} + \mathcal{A}_{4,6}^{[3-1]} + \mathcal{A}_{6,8}^{[2-3]}, \\ \mathcal{A}(\gamma_L^a) &= \mathcal{A}_{1,2}^{[1]} + \mathcal{A}_{2,4}^{[3-1]} + \mathcal{A}_{4,6}^{[1-2]} + \mathcal{A}_{6,8}^{[1-2]}, \\ \mathcal{A}(\gamma_L^b) &= \mathcal{A}_{1,2}^{[2]} + \mathcal{A}_{2,4}^{[2-3]} + \mathcal{A}_{4,6}^{[2-3]} + \mathcal{A}_{6,8}^{[3-1]}, \\ \mathcal{A}(\gamma_U^a) &= \mathcal{A}_{8,7}^{[2]} + \mathcal{A}_{7,5}^{[3]} + \mathcal{A}_{5,3}^{[3]} + \mathcal{A}_{3,1}^{[1]}, \\ \mathcal{A}(\gamma_U^c) &= \mathcal{A}_{8,7}^{[1]} + \mathcal{A}_{7,5}^{[1]} + \mathcal{A}_{5,3}^{[2]} + \mathcal{A}_{3,1}^{[2]}, \\ \mathcal{A}(\gamma_U^b) &= \mathcal{A}_{8,7}^{[3]} + \mathcal{A}_{7,5}^{[2]} + \mathcal{A}_{5,3}^{[1]} + \mathcal{A}_{1,3}^{[3]}, \end{aligned}$$

cf. (55) and (56), then

$$\begin{aligned} \mathcal{A}(\gamma_{\infty}^{c-a}) &= \mathcal{A}(\gamma_L^c) + \mathcal{A}(\gamma_U^a), \\ \mathcal{A}(\gamma_{\infty}^{a-c}) &= \mathcal{A}(\gamma_L^a) + \mathcal{A}(\gamma_U^c), \end{aligned}$$

$$\mathcal{A}(\gamma_\infty^{b-b}) = \mathcal{A}(\gamma_L^b) + \mathcal{A}(\gamma_U^b).$$

$\mathcal{A}(\gamma_L^c)$ can be used to reach the vicinity of B_8 on Sheet a, and $\mathcal{A}(\gamma_\infty^{c-a})$ to reach the vicinity of B_1 on Sheet a. By $\mathcal{A}(\gamma_\infty^{c-a}) + \mathcal{A}(\gamma_\infty^{a-c})$ Sheet b can be reached in the vicinity of B_1 , by $\mathcal{A}(\gamma_\infty^{c-a}) + \mathcal{A}(\gamma_\infty^{a-c}) + \mathcal{A}(\gamma_L^b)$ the vicinity of B_8 on Sheet b. Then

$$\begin{aligned} \mathcal{A}(P_1) &= \mathcal{A}_{0-,1}^{[3]} + \mathcal{A}(\gamma_\infty^{c-a}) + \mathcal{A}_{1,3}^{[1]} + \int_{B_3}^{P_1} du^{[1]}, \\ \mathcal{A}(P_2) &= \mathcal{A}_{0-,1}^{[3]} + \mathcal{A}(\gamma_\infty^{c-a}) + \mathcal{A}(\gamma_\infty^{a-c}) + \mathcal{A}_{1,2}^{[2]} + \mathcal{A}_{2,4}^{[2-3]} + \mathcal{A}_{4,6}^{[2-3]} + \mathcal{A}_{6,5}^{[3-1]} + \int_{B_5}^{P_2} du^{[1]}, \\ \mathcal{A}(P_3) &= \mathcal{A}_{0-,1}^{[3]} + \mathcal{A}(\gamma_\infty^{c-a}) + \mathcal{A}_{1,2}^{[1]} + \mathcal{A}_{2,4}^{[3-1]} + \mathcal{A}_{4,6}^{[1-2]} + \int_{B_6}^{P_3} du^{[1]}, \end{aligned}$$

which produce an Abel image congruent to (58), namely

$$(60) \quad u(D) = \sum_{i=1}^3 \mathcal{A}(P_i) \approx \begin{pmatrix} -0.546310 + 0.440673i \\ 0.496998 - 0.233192i \\ 0.028495 - 0.067950i \end{pmatrix},$$

and the same values of \wp -functions (64).

On the other hand, a solution of the Jacobi inversion problem on a (3, 4)-curve (50) is given by the system

$$(61a) \quad \mathcal{R}_6(x, y; u) = x^2 - y\wp_{1,1}(u) - x\wp_{1,2}(u) - \wp_{1,5}(u),$$

$$(61b) \quad \begin{aligned} \mathcal{R}_7(x, y; u) &= 2xy + y(\wp_{1,1,1}(u) - \wp_{1,2}(u)) \\ &\quad + x(\wp_{1,1,2}(u) - \wp_{2,2}(u)) + (\wp_{1,1,5}(u) - \wp_{2,5}(u)). \end{aligned}$$

Given a divisor D , the two entire rational functions \mathcal{R}_6 and \mathcal{R}_7 can be obtained as determinants of the two matrices, respectively,

$$\begin{aligned} \mathcal{R}_6(D) &= \begin{pmatrix} 1 & x & y & x^2 \\ 1 & x_i & y_i & x_i^2 \end{pmatrix}_{i=1}^3, \\ \mathcal{R}_7(D) &= \begin{pmatrix} 1 & x & y & xy \\ 1 & x_i & y_i & x_i y_i \end{pmatrix}_{i=1}^3, \end{aligned}$$

where (x_i, y_i) denote coordinates of P_i . After a proper normalization, we have

$$\begin{aligned} \mathcal{R}_8(x, y; u(D)) &= x^2 - (0.059654 + 1.020925i)y \\ &\quad + (0.793416 - 0.889005i)x - 0.885372 + 3.089764i, \\ \mathcal{R}_9(x, y; u(D)) &= 2xy - (1.363160 - 2.654511i)y \\ &\quad - (3.325329 - 1.368120i)x + 9.157983 - 11.098669i. \end{aligned}$$

Coefficients of the two functions coincide with those expressed in terms of \wp -functions on D from (59) with an accuracy of 10^{-13} .

6.2. Example 3b. Let D be slightly modified by choosing points with the same x -coordinates, but located on different sheets, namely

$$\begin{aligned} P_1 &= (e_3 - 0.5 - 0.5i, y_2(e_3 - 0.5 - 0.5i)) \\ &\approx (-1.679223 + 0.434455i, -3.855009 + 0.446784i), \end{aligned}$$

$$\begin{aligned} P_2 &= (e_5 + 0.5 - 1.5i, y_3(e_5 + 0.5 - 1.5i)) \\ &\approx (0.068268 + 0.702564i, -0.916997 - 0.935049i), \end{aligned}$$

$$\begin{aligned} P_3 &= (e_6 + 1, y_3(e_6 + 1)) \\ &\approx (1.499118 - 1.575269i, 5.701625 - 3.318255i). \end{aligned}$$

The points P_1 and P_3 are located on Sheet b, and P_2 on Sheet a. Let P_1 and P_3 on Sheet b be reached through the cut between B_4 and B_5 , and P_2 on Sheet a through the cut between B_6 and B_7 , see fig. 11(b). Actually,

$$\begin{aligned} \mathcal{A}(P_1) &= \mathcal{A}_{0-1}^{[3]} + \mathcal{A}_{1,3}^{[3]} + \mathcal{A}_{3,5}^{[1]} + \mathcal{A}_{5,3}^{[2]} + \int_{(e_3, y_2(e_3))}^{P_1} du^{[2]}, \\ \mathcal{A}(P_2) &= \mathcal{A}_{0-1}^{[3]} + \mathcal{A}_{1,3}^{[3]} + \mathcal{A}_{3,5}^{[1]} + \mathcal{A}_{5,7}^{[2]} + \mathcal{A}_{7,5}^{[3]} + \int_{(e_5, y_3(e_5))}^{P_2} du^{[3]}, \\ \mathcal{A}(P_3) &= \mathcal{A}_{0-1}^{[3]} + \mathcal{A}_{1,2}^{[3]} + \mathcal{A}_{2,4}^{[1-2]} + \mathcal{A}_{4,6}^{[2-3]} + \int_{B_6}^{P_3} du^{[3]}, \end{aligned}$$

The Abel image of D is

$$(63) \quad u(D) = \sum_{i=1}^3 \mathcal{A}(P_i) \approx \begin{pmatrix} -0.421105 - 2.303962i \\ -1.319230 - 1.997581i \\ -0.176345 + 0.125109i \end{pmatrix},$$

and \wp -functions acquire the following values

$$\begin{aligned} \wp_{1,1}(u(D)) &\approx -0.497171 - 1.306218i, \\ \wp_{1,2}(u(D)) &\approx 0.485105 + 2.618402i, \\ \wp_{1,5}(u(D)) &\approx 2.083016 - 2.086324i, \\ \wp_{2,2}(u(D)) &\approx -2.356414 + 10.869587i, \\ \wp_{2,5}(u(D)) &\approx 15.590831 + 2.902800i, \\ \wp_{1,1,1}(u(D)) &\approx 1.678988 + 8.731706i, \\ \wp_{1,1,2}(u(D)) &\approx -4.377331 - 0.119524i, \\ \wp_{1,1,5}(u(D)) &\approx 2.198126 + 13.211222i. \end{aligned} \quad (64)$$

On the other hand, the given divisor D is a solution of the system, cf. (61)

$$\begin{aligned} \mathcal{R}_8(x, y; u(D)) &= x^2 + (0.497171 + 1.306218i)y \\ &\quad - (0.485105 + 2.618402i)x - 2.083016 + 2.086324i, \\ \mathcal{R}_9(x, y; u(D)) &= 2xy + (1.193883 + 6.113304i)y \\ &\quad - (2.020917 + 10.989112i)x - 13.392705 + 10.308422i. \end{aligned}$$

Coefficients obtained from the divisor directly, and from the values (64) of \wp -functions on D coincide with an accuracy of 10^{-9} .

7. ACKNOWLEDGMENTS

The present paper was inspired by S. Matsutani, who expressed an active interest into analytical computation of \wp -functions in Mathematica.

REFERENCES

- [1] Agostini D., Chua L., Computing theta functions with Julia, *Journal of Software for Algebra and Geometry* **11** (2021), pp. 41–51
- [2] Baker H.F., *Abelian functions: Abel's theorem and the allied theory of theta functions*, Cambridge, University press, Cambridge, 1897.
- [3] Baker H.F., *Multiply periodic functions*, Cambridge Univ. Press, Cambridge, 1907.
- [4] Belokolos E. D., Bobenko A. I., Enolski V. Z., Its A. R., Matveev. V.B., *Algebro-geometric approach to nonlinear integrable equations*, Springer-Verlag, 1994
- [5] Bernatska J., General derivative Thomae formula for singular half-periods, *Lett. Math. Phys.* (2020), arXiv:1904.09333 [math.AG]
- [6] Bernatska J., Reality conditions for the KdV equation and exact quasi-periodic solutions in finite phase spaces, preprint, arXiv:2312.10859.
- [7] Bernatska J., Leykin D. Solution of the Jacobi inversion problem on non-hyperelliptic curves, *Lett. Math. Phys.* **113** 110 (2023); arXiv:2212.14492
- [8] Bolza O. Ueber die Reduction hyperelliptischer Integrale erster Ordnung und erster Gattung auf elliptische durch eine Transformation vierten Grades, *Math. Ann.* **28**:3 (1887) pp. 447–456.
- [9] Buchstaber V. M., Enolskii V. Z., Leykin D. V., *Rational analogs of abelian functions*, *Functional Analysis and Its Applications*, **33**:2 (1999) pp. 83–94.
- [10] Buchstaber V. M., Enolskii V. Z., and Leykin D. V., *Hyperelliptic Kleinian Functions and Applications*, preprint ESI 380 (1996), Vienna
- [11] Buchstaber V. M., Enolskii V. Z., Leykin D. V., Uniformization of Jacobi varieties of trigonal curves and nonlinear differential equations, *Functional Analysis and Its Applications* **34** (2000) pp. 159–171
- [12] Deconinck B., van Hoeij M., Computing Riemann matrices of algebraic curves, *Physica D* **152–153** (2001), pp. 28–46
- [13] Deconinck B., Patterson M. S., Computing with plane algebraic curves and Riemann surfaces: The algorithms of the Maple package “Algcures” in Computational approach to Riemann surfaces (Lect. Notes Math. Vol. 2013), eds. Bobenko A. I., Klein C., Berlin: Springer, 2011,
- [14] Dubrovin B. A., Theta functions and non-linear equations, *Russ. Math. Surv.* **36**:2 (1981), pp. 11–80
- [15] Enolski V.Z., Richter P.H. Periods of hyperelliptic integrals expressed in terms of θ -constants by means of Thomae formulae. *Phil. Trans. London Math. Soc. A* (2008), **366**, pp.1005–1024
- [16] Fay J. D., *Theta functions on Riemann surfaces*, Lectures Notes in Mathematics (Berlin), vol. 352, Springer, 1973.
- [17] Frauendiener J., Klein C., Hyperelliptic theta-functions and spectral methods, *Journal of Computational and Applied Mathematics* **167** (2004), pp.193–218.
- [18] Frauendiener J., Klein C., Hyperelliptic theta-functions and spectral methods: KdV and KP solutions, *Lett. Math. Phys.* **76**, (2006) pp. 249–267.
- [19] Kalla C., Klein C., On the numerical evaluation of algebro-geometric solutions to integrable equations, *Nonlinearity*, **25** (2012), pp. 569–596.
- [20] Matsutani S., Previato E., An algebro-geometric model for the shape of supercoiled DNA, *Physica D*, (2022) **430**, 133073
- [21] Matsutani S., A graphical representation of hyperelliptic KdV solutions, arXiv:2310.14656